

University of Texas Rio Grande Valley

ScholarWorks @ UTRGV

Theses and Dissertations

5-2022

Evaluation of Accelerated Testing Methods to Predict the Effects of Chemical Exposure on Mechanical Properties of Polyester Composites in Municipal Wastewater Service

Roberto A. Garcia

The University of Texas Rio Grande Valley

Follow this and additional works at: <https://scholarworks.utrgv.edu/etd>



Part of the [Mechanical Engineering Commons](#)

Recommended Citation

Garcia, Roberto A., "Evaluation of Accelerated Testing Methods to Predict the Effects of Chemical Exposure on Mechanical Properties of Polyester Composites in Municipal Wastewater Service" (2022). *Theses and Dissertations*. 873.

<https://scholarworks.utrgv.edu/etd/873>

This Thesis is brought to you for free and open access by ScholarWorks @ UTRGV. It has been accepted for inclusion in Theses and Dissertations by an authorized administrator of ScholarWorks @ UTRGV. For more information, please contact justin.white@utrgv.edu, william.flores01@utrgv.edu.

EVALUATION OF ACCELERATED TESTING METHODS TO PREDICT THE EFFECTS
OF CHEMICAL EXPOSURE ON MECHANICAL PROPERTIES OF POLYESTER
COMPOSITES IN MUNICIPAL WASTEWATER SERVICE

A Thesis

by

ROBERTO A. GARCIA

Submitted in Partial Fulfillment of the
Requirements for the Degree of
MASTER OF SCIENCE IN ENGINEERING

Major Subject: Mechanical Engineering

The University of Texas Rio Grande Valley

May 2022

EVALUATION OF ACCELERATED TESTING METHODS TO PREDICT THE EFFECTS
OF CHEMICAL EXPOSURE ON MECHANICAL PROPERTIES OF POLYESTER
COMPOSITES IN MUNICIPAL WASTEWATER SERVICE

A Thesis
by
ROBERTO A. GARCIA

COMMITTEE MEMBERS

Dr. Constantine Tarawneh
Co-Chair of Committee

Dr. Robert Jones
Co-Chair of Committee

Dr. Arturo Fuentes
Committee Member

May 2022

Copyright 2022 Roberto A. Garcia

All Rights Reserved

ABSTRACT

Garcia, Roberto A., Evaluation of Accelerated Testing Methods to Predict the Effects of Chemical Exposure on Mechanical Properties of Polyester Composites in Municipal Wastewater Service. Master of Science in Engineering (MSE), May, 2022, 72 pp., 25 tables, 54 figures, references, 29 titles.

There is a need to replace traditional iron manhole covers with fiber reinforced polymer alternatives that perform similarly while also introducing several advantages. Commercial providers have achieved this by manufacturing polymer manhole covers using high-speed, high-pressure compression molding, or resin transfer molding, to produce lightweight, long-lasting, corrosion resistant covers. These composite covers have been approved for use by the Texas Department of Transportation (TXDOT, pronounced tex-dot) in roadway zones. Despite positive results with this material, more testing and validation is required for use in environments with highly corrosive elements such as sewage and waste processing plants. In these situations, the polymer manhole covers will be exposed to high amounts of hydrogen sulfide - a gas yielded by microbiology from human waste which interacts with moisture to produce sulfuric acid. The testing conducted in this body of work is used to determine how the structural integrity of the manhole cover will perform when exposed to a range of acidity levels, or varying exposure periods in wastewater service. Mechanical properties will be tested to observe the effects of different levels of corrosive exposure on the tested material. This investigation will serve to prove whether this new product is suitable for use in highly corrosive environments.

DEDICATION

This thesis and the completion of my graduate studies are dedicated to my family, which has supported me throughout my lengthy academic career with unconditional love and a level of faith that often exceeded my own. My mother, Sonia Martinez, who raised me with the strength to shoulder any burden with a smile. My late father, Robert John Garcia, who taught me the importance of being a gentleman and a scholar in leading by example. My sisters, who always seem to double down in the face of adversity, meeting challenges with grit and grim determination. And Gio, who helped me be truer to myself.

ACKNOWLEDGMENTS

I would like to thank the UTCRS team, for being a second family focused on mutual success and mutual reliability, and for lending a helping hand when I was reluctant to ask for one.

I would like to thank Dr. Jones for his wisdom in matters that weren't strictly academic, and for pushing me when I needed it, and kicking me when I needed it even more.

A special thank you to Dr. Constantine Tarawneh for his enduring patience in mentoring and nurturing everyone in his selfless pursuit of their best interest. I would not be where I am today without his talent for drawing out the potential in his students. Truly, he was equal parts strict, kind, and fair, not unlike a caring father figure.

Gratitude to Hector Arteaga and the other folks in the machine shop who helped me safely develop fixtures and filled in the holes in my experience with guided instruction.

And a nod to Dr. Turner, Dr. Fuentes, Jazmin Ley, Samantha Ramirez, Jesse Sanchez, and all those others who believed in my capacity for more

TABLE OF CONTENTS

	Page
ABSTRACT.....	iii
DEDICATION.....	iv
ACKNOWLEDGMENTS	v
TABLE OF CONTENTS.....	vi
LIST OF TABLES	vii
LIST OF FIGURES	viii
CHAPTER I. BACKGROUND AND INTRODUCTION.....	1
CHAPTER II. LITERATURE REVIEW	6
CHAPTER III. METHODOLOGY	12
CHAPTER IV. RESULTS AND ANALYSIS	30
CHAPTER V. CONCLUSIONS AND FUTURE WORK.....	53
REFERENCES	56
APPENDIX.....	59
BIOGRAPHICAL SKETCH	70

LIST OF TABLES

	Page
Table 1: Material Properties for the unsaturated polyester composite samples.....	13
Table 2: Concentrations for Immersion Tests.....	22
Table 3: Concentration Summary for Hydrogen Sulfide Gas Readings.....	32
Table 4: Temperature Summary for Hydrogen Sulfide Gas Readings	32
Table 5: Average Flexural Test Results of Laboratory Corrosion Conditions	34
Table 6: ANOVA Test for Young’s Modulus in Laboratory Immersion Test	35
Table 7: Average Flexural Test Results for All Plate-Derived Coupons.....	37
Table 8: Average Flexural Test Results for All Coupons.....	37
Table 9: ANOVA Test for Plate Young’s Modulus in Field Test	38
Table 10: ANOVA Test for Plate Flexural Stress at Break in Field Test.....	39
Table 11: ANOVA Test for Plate Strain at Break in Field Test	40
Table 12: ANOVA Test for Plate Energy at Break in Field Test	41
Table 13: ANOVA Test for Coupon Young’s Modulus in Field Test	42
Table 14: ANOVA Test for Coupon Flexural Stress at Break in Field Test	43
Table 15: ANOVA Test for Coupon Strain at Break in Field Test	44
Table 16: ANOVA Test for Coupon Energy at Break in Field Test	45
Table 17: Changes in Coupon Mass after Exposure.....	47
Table 18: Rockwell Hardness Tests for FRC Coupons Exposed to Field Conditions.....	48
Table 19: Gray Iron Tensile Test Results	49
Table 20: Properties Used to Calculate Corrosion Rate for Iron Tensile Specimen	49
Table 21: Experimental Corrosion Rates for Mild Steel [28].....	50
Table 22: SRB Concentrations for Varying Mediums.....	51
Table 23: ANOVA Immersion Test Flexural Stress.....	60
Table 24: ANOVA Immersion Test Flexural Strain.....	61
Table 25: ANOVA Immersion Test Energy at Break.....	61

LIST OF FIGURES

	Page
Figure 1: MIC of concrete in sewer environments [7].....	7
Figure 2: Polymer-solvent interface. [21]	9
Figure 3: Plate and Coupon Sample Size Comparisons.....	15
Figure 4: Composite Plates and Iron Bars Suspended in Test Environment	16
Figure 5: OdaLog L2 Gas Logger.....	17
Figure 6: Three-Point Bending Test on Instron 5966	18
Figure 7: Three-Point Bending Test Schematic and Corresponding Moment (M), Shear (Q), and Deflection (W) graphs [http://commons.wikimedia.org/wiki/File:SimpSuppBeamPointLoad.svg]	19
Figure 8: Coupon in Flexural Stress During Bending Test.....	20
Figure 9: Swollen Polymer Coupon Matrix.....	21
Figure 10: Acid Immersion Tests – Polyester Coupons	21
Figure 11: Acid Immersion Tests - Iron Tensile Coupons	22
Figure 12: pH testing the condensate.....	23
Figure 13: Iron Bar Tensile Tests	24
Figure 14: Iron Tensile Specimens – Exposed for 8 months (Left); Unexposed (Right)	24
Figure 15: HRL Hardness Testing	25
Figure 16: 3M SRB Detection Pouch Quantitation Estimates.....	26
Figure 17: Rapid SRB Detection of water beneath FRC samples	27
Figure 18: Rapid SRB Detection of Iron Sample (Left), and of Composite Plate (Right)	28
Figure 19: SOB Test Vials – Composite Sample (Left), Control Sample (Middle), and Iron Sample (Right).....	29
Figure 20: H ₂ S Concentration and Temperature October 28 th to November 4 th	30
Figure 21: H ₂ S Concentration and Temperature November 25 th to December 2 nd	31
Figure 22: H ₂ S Concentration and Temperature March 24 th to March 31 st	31
Figure 23: H ₂ S Concentration and Temperature April 22 nd to April 29 th	31
Figure 24: FRC Coupons Exposed to [20 wt%] Sulfuric Acid for 14 days.....	33
Figure 25: FRC Coupons Exposed to [30 wt%] Sulfuric Acid for 14 days.....	33
Figure 26: FRC Coupons Exposed to [50 wt%] Sulfuric Acid for 14 days.....	33
Figure 27: Flexural Test for Coupon Specimens 1 to 3	36
Figure 28: Field Testing - Plate Young's Modulus versus Exposure Time.....	38
Figure 29: Field Testing - Plate Flexural Stress at Break versus Exposure Time	39
Figure 30: Field Testing - Plate Strain at Break versus Exposure Time.....	40

Figure 31: Field Testing - Plate Energy at Break versus Exposure Time.....	41
Figure 32: Field Testing - Coupon Young's Modulus versus Exposure Time	42
Figure 33: Field Testing - Coupon Flexural Stress at Break versus Exposure Time.....	43
Figure 34: Field Testing - Coupon Strain at Break versus Exposure Time	44
Figure 35: Field Testing - Coupon Energy at Break versus Exposure Time	45
Figure 36: 3M Rapid SRB Tests for Iron (Left), FRC (Middle), Wastewater (Right)	51
Figure 37: SOB Bacteria Test Results: FRC (Left), Control (Middle), Iron (Right)	52
Figure 38: Gas Logger H ₂ S Data in Test Site – overlaid	60
Figure 39: Flexural Tests for Coupons 4 to 6	62
Figure 40: Flexural Tests for Coupons 7 to 9	62
Figure 41: Flexural Tests for Coupons 10 to 12	63
Figure 42: Flexural Tests for Coupons 13 to 16	63
Figure 43: Flexural Tests for Coupons 17 to 20	64
Figure 44: Flexural Tests for Coupons 21 to 24	64
Figure 45: Flexural Tests for Coupons 25 to 28	65
Figure 46: Flexural Tests for Coupons 29 to 32	65
Figure 47: Flexural Tests for Plate 1 – 4 specimens	66
Figure 48: Flexural Tests for Plate 2 – 3 specimens	66
Figure 49: Flexural Tests for Plate 3 – 3 specimens	67
Figure 50: Flexural Tests for Plate 4 – 3 specimens	67
Figure 51: Flexural Tests for Plate 5 – 3 specimens	68
Figure 52: Flexural Tests for Plate 6 – 3 specimens	68
Figure 53: Flexural Tests for Plate 7 – 3 specimens	69
Figure 54: Flexural Tests for Plate 8 – 4 specimens	69

CHAPTER I

BACKGROUND AND INTRODUCTION

Wastewater treatment alleviates the otherwise heavy influence concentrated populations can have on the environment, and repurposes waste elements for irrigation, industrial consumption, and the supplementation of ecological water. Municipalities in the United States tend to rely on either combined sewer systems or separate sanitary sewers for channeling waste. As the name implies, combined sewer systems transport stormwater and sanitary sewage in a single-pipe system, whereas the separate sanitary sewers collect only wastewater and do not provide the drainage necessary for excess runoff from precipitation events. Combined sewers may overflow during extended wet weather conditions, which heavily discouraged their construction since the first half of the 20th century [1]. Separate sanitary sewer systems are heavily prone to biological corrosion processes because of higher sewage concentrations than those found in combined sewers. Concrete and other iron-containing materials are more susceptible to this type of corrosion and will degrade faster than if attacked by ordinary oxidizing environments.

The key to this accelerated corrosion in sanitary sewer systems is biological in origin, where bacteria attach to a material surface and subsequently form a biofilm which can deteriorate that surface by forming a local environment that is harmful to the physical or chemical properties of the material [2][3]. This biological corrosion process is called microbiologically induced corrosion (MIC) [4]. Sulfate reducing bacteria (SRB) and sulfate oxidizing bacteria (SOB) are

some of the most reported and studied bacteria regarding MIC. They have been proven to influence the corrosion of metals and metallic materials, especially ferrous alloys, when present in the biofilm that tends to form on these materials. SRB and SOB are usually associated visually with pitting, a form of corrosion attack that forms small grooves and divots on the surface of the material. In anaerobic MIC, oxidants like sulfates accept electrons released by iron oxidation. Corrosion caused by SRB requires a neutral pH and a lack of oxygen, with corrosion products including iron sulfides. The *Desulfovibrio* SRB species are aerotolerant and can survive in O₂-rich environments with limited growth. Corrosion caused by SOB is an aerobic process with a lower pH and a thus stronger acidic attack. It is important to employ corrosion resistant materials and coatings such as stainless steel or high-grade thermoplastics in water treatment systems where this type of degradation is a factor.

Composite materials offer a potential solution to the challenge of operating in a MIC prone environment. Fiber reinforced composites (FRCs) are comprised of a homogeneous polymer matrix that surrounds and protects high strength and stiffness reinforcing fibers. The fibers are the main load bearing portion of the composite while the polymer matrix acts as a binding agent, keeping fibers in place and transferring stresses between them. There are various advantages to using fiber reinforced polymers as a material for manhole covers as opposed to iron. Using a polymer substitute will reduce theft, as the material is a thermoset and more difficult to recycle and repurpose unlike iron which can be sold to recyclers. The material is easier to lift and transport, which will reduce shipping costs and worker injuries. The material is also inherently immune to oxidation, where iron would rust quickly in humid environments.

There are multiple failure modes possible in fiber composites. The mode most relevant to this work is caused by acidic corrosion. Acidic corrosion removes reinforcing material from

the composite, or penetrates and degrades the polymer matrix, which causes the structural integrity of the FRC to become compromised. Other failure modes include delamination, where the transverse forces between the laminated layers of the composite overcome the adhesive forces keeping the layers attached together, and matrix microcracking.

The focus of this body of work is on acidic corrosion and its effect on the FRC along with an evaluation of its performance as a replacement for traditional iron manhole covers. The intent is to determine if a polyester FRC manhole cover can successfully replace a standard iron manhole cover in terms of strength and corrosion resistance. Laboratory corrosion tests commonly used to quantify materials include the chemical resistance test (also known as the pickle jar test), the hot wall test, and the salt spray test.

The hot wall test is used to evaluate situations where metal vessels are hotter than the surrounding bulk solutions and is commonly used when corrosion rates are affected by high temperatures. The salt spray test is an accelerated corrosion test used to measure the corrosion resistance of materials exposed to salt spray or salt fogs at high temperatures.

For this work, testing was done both in the field, on the premises of a waste processing plant, and in the laboratory via a chemical resistance test. The chemical resistance or pickle jar test aimed to simulate field conditions in an accelerated process by fully immersing specimens in diluted acid inside of a sealed container and at a set temperature. Multiple specimens were tested in both field and laboratory tests over a period of twelve months to gauge the impact of the corrosive environment on the strength and durability of the FRC material.

The main objective of the data obtained from this work is to find a correlation between mass lost or material strength and exposure time to determine whether the polymer composite would be safe for long term use.

The material tested is an E-glass fiber reinforced polyester polymer with a filler of Calcium Carbonate particles. For the purposes of this research, CAP has provided sample plates and strips that are representative of the material found in their manhole covers. These samples were used for all testing procedures carried out in lieu of the larger full-size manhole cover. The size and weight of the manhole cover made field testing impractical.

Field testing was conducted by suspending samples above churning wastewater and concurrently measuring the properties of that environment so that a representative laboratory setup could be created. The microbiology involved in human waste, sulfate reducing bacteria *Desulfovibrio sp. genera*, would produce a highly concentrated Hydrogen sulfide (H_2S) gas that aerobic bacteria above the waterline would consume and oxidize to produce sulfuric acid. Replicating this phenomenon, preliminary laboratory setups involved a heavily diluted pickle jar test (5% or 1M of Sulfuric Acid), and an undiluted pickle jar test (96% or 18.4M Sulfuric Acid). Samples immersed in the diluted pickle jar were completely unaffected, whereas those immersed in the undiluted pickle jar lost all structural integrity and were affected by swelling and dissolution before being reduced to sludge. These tests demonstrated that the FRC material was indeed susceptible to an acid-based attack.

The corrosion science regarded in the literature review consistently points to sulfate reducing biofilms as the cause for corrosion in concrete and steel. The presence of a biofilm on the composite samples would reveal the extent to which the samples were affected by corrosion.

A linear trend between the ultimate yield strength and exposure time of the samples would also indirectly show the extent to which samples were corroded, or if a year is too short an exposure period for the given material, in the given environment, to show a decline in material strength.

CHAPTER II

LITERATURE REVIEW

The microbiologically induced corrosion (MIC) in wastewater systems is a multi-stage process severely deteriorating concrete, iron, steel, and other iron-based metals, alloys, and products. Early studies concerning the corrosion of concrete sewer pipes, dating back over a century, accepted sulfuric acid as the corrosive agent, with the relationship to hydrogen sulfide gas and microbiology being discovered years later [5]. The events and processes involved in the MIC of concrete sewer systems have since been debated in the scientific community and a consensus was established by M. Wu et al. [6] and can be summarized as follows:

1. Aqueous hydrogen sulfide $\text{H}_2\text{S}_{(\text{aq})}$ forms in the solution: anaerobic sulfate reducing bacteria (SRB), such as *Desulfovibrio Desulfuricans*, residing in biofilms, below the waterline or in the slime layer, convert sulfates in the waste stream to $\text{H}_2\text{S}_{(\text{aq})}$.
2. Build up and radiation of $\text{H}_2\text{S}_{(\text{g})}$: the gas phase emerges to the space above the waterline, which can be aided by turbulence.
3. Sulfuric acid generation $\text{H}_2\text{SO}_{4(\text{aq})}$: aerobic sulfur oxidizing bacteria (SOB), such as *Thiobacillus Ferrooxidans*, present above the waterline on concrete surfaces produce sulfuric acid, which accumulates under a biofilm.
4. Corrosion and deterioration: the generated sulfuric acid, along with other possible biogenic acids, degrades the concrete matrix and disintegrates the material, as evidenced by pitting.

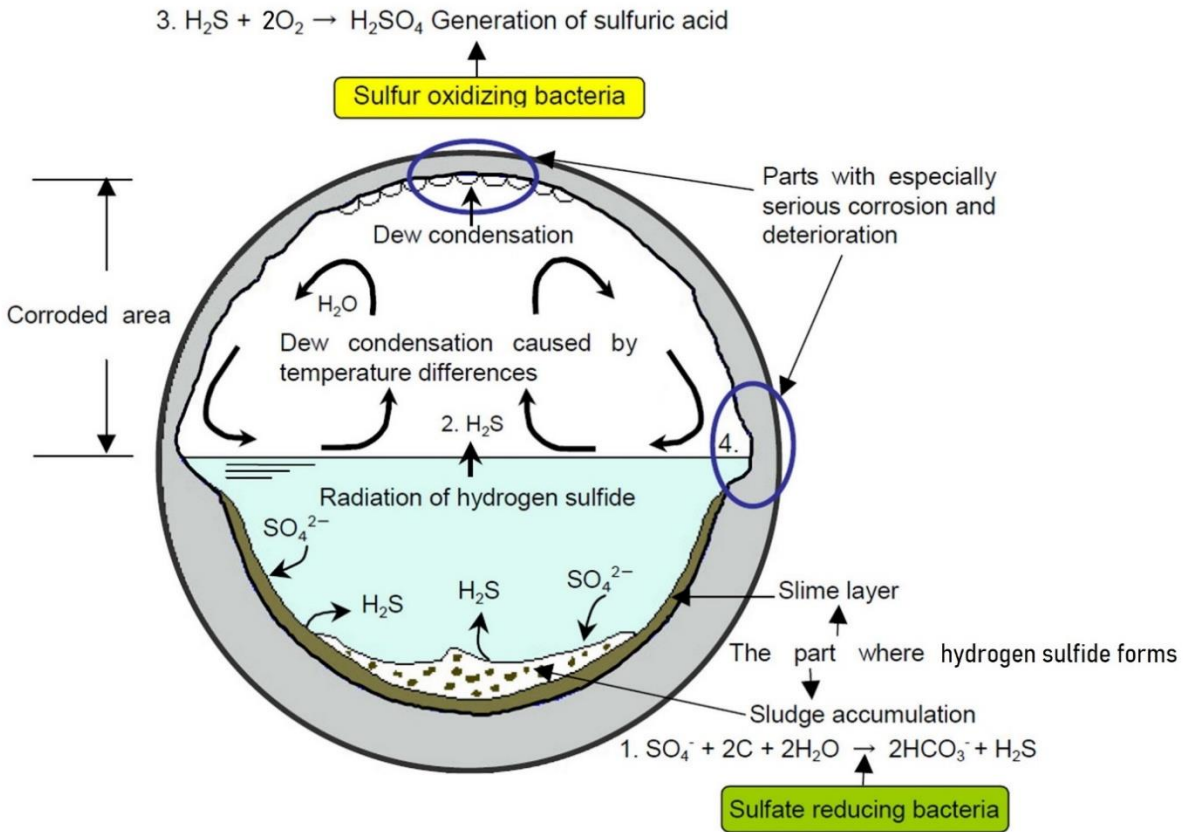


Figure 1: MIC of concrete in sewer environments [7]

In biofilm formation, the process of initial bacterial attachment is affected by factors that include the physio-chemical properties of microorganisms, the microstructure of the attachment surface, and environmental conditions [8]-[12]. Beech and Gaylarde [15] have identified extracellular polymeric substance (EPS) as crucial in the initial attachment of *Pseudomonas fluorescens* and *Desulfovibrio desulfuricans* to mild steel surfaces. It has also been found that lipopolysaccharides (LPS) in the outer membrane of gram-negative cells like SRB genus *Desulfovibrio*, interact specifically with ferrous $[\text{Fe}(\text{II})]$ ions [14]. These interactions could affect both the initial attachment of the bacteria and the ensuing corrosion of ferrous metals in an aqueous environment [15]. Preventing SRB from attaching to a metal surface has proven to

reduce the rate of corrosion of that metal. King *et. al.* [16]-[17] have shown that the concentration of ferrous ions in the test media is directly proportional to the rate of corrosion of mild steel.

Thiobacilli are one of the best-known oxidizers of iron and sulfur. The *Thiobacillus Ferrooxidans* bacterium can use reduced iron ions (Fe^{2+}) as a source of energy. However, the bacterial influence on the aerobic corrosion of iron is still the subject of some controversy. There are many variables associated with different types of bacteria or environmental conditions, such as ion concentration, metallic impurities, pH, or ionic strength, that make definitive conclusions difficult to verify [18]. A study by W.K. Choi [19] observed the rapid corrosion of different steels submerged in a nutrient solution without the addition of ferrous ions. The highest rate of corrosion was exhibited in the sample with the greatest sulfur content (416 Stainless Steel, 0.32% Sulfur) which is explained by the oxidation of elemental sulfur to sulfuric acid by means of bacterial activity. A study by B.J. Little and P.A. Wagner [20] exposed iron-oxidizing bacteria to a stainless steel electrode with and without the presence of ferrous ions in the solution. The authors reported there was no noticeable corrosion due to bacterial activity without the addition of ferrous ions.

Iron and iron-based materials corrode by electrochemical reactions, whereas polymeric materials are affected by physiochemical processes [21]. Polymeric materials degrade through swelling, dissolution, and bond rupture caused by chemical reaction, heat, moisture, ultraviolet (UV) radiation, thermal cycling, and mechanical fatigue.

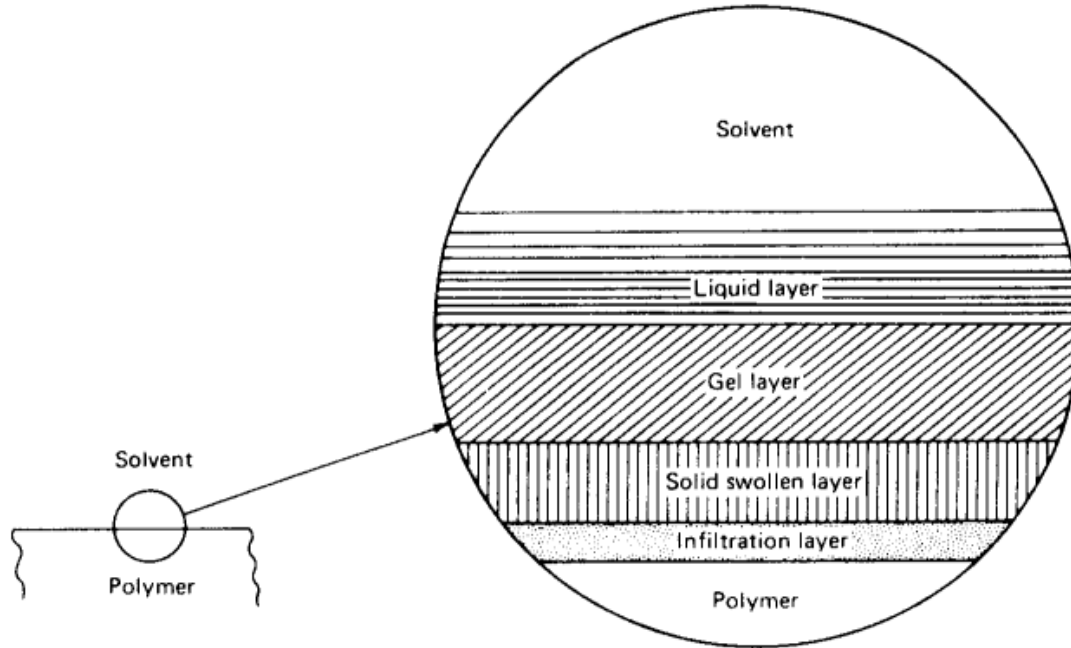


Figure 2: Polymer-solvent interface. [21]

The liquid and solid phases form the outer layers of a multilayer interface where the polymer is penetrated by small quantities of the solvent, which forms a layer of infiltration with altered physical properties. Swollen solvent-rich solid and gel layers are usually present above the infiltration layer. A liquid layer with a concentration gradient reaches out into the solution. Not all the layers shown in Figure 2 are observed during liquid attack of polymers. In some cases, the swollen solid layer has its mechanical properties altered, and can crack under internal stresses [21].

Epoxy chemical resistance is generally slightly superior to that of polyesters. Carbon-epoxy composites can absorb moisture which will affect their thermophysical, mechanical, and chemical characteristics by plasticization and hydrolysis [22]. These changes can reduce the elastic modulus of the material [23]. The physical, chemical, and mechanical degradation of an IM7/997 fiber reinforced composite (FRC) was the subject of a recent study, following exposure to water vapor and UV radiation [24]. It was found that the synergy of these two conditions

cause moderate microcracking and erosion of the epoxy matrix. Cyclic loading is the most common failure mode observed for composite materials in service, and the effects can be compounded with the addition of corrosive environmental conditions [25]. The internal damage accumulated during cyclic loading has a higher degree of complexity in composites than that in metals or ceramics, as the internal microstructure of composites experiences various forms of damage that include delamination, matrix cracking, debonding, fiber breakage, and ply failure. The cumulative result of these damage modes is often initialized by numerous small cracks, as opposed to the propagation of a single predominant crack as seen with metals. Exposure to corrosive environments will lead to physical and chemical degradation that affect standard material properties and provide concentrated damage initiation sites where damage is accrued under fatigue loading [25].

Feng *et. al.* [26] studied the effects of corrosive environments on properties of pultruded glass fiber reinforced polymer (GFRP) plates. The reinforcement of these plates consisted of five layers: a middle layer of a glass fiber mat, two surrounding layers of woven roving glass fiber, and two outermost layers of the same glass fiber mat as the middle layer. Epoxy resin was used for the matrix to offer corrosion resistance and adhesion. Samples were cut and exposed to alkaline, saline, and acidic solutions of different concentrations at 60°C (140°F) and 90°C (194°F). Results indicated that flexural strength decreased with increased exposure time, with an even more drastic effect for higher acid concentrations and higher acid temperatures. The substances used for exposure included H₂SO₄, NaOH, and NaCl with saltwater having no discernible effect. The researchers exposed these samples for 7, 15, 30, and a maximum of 90 days. The conditions for the H₂SO₄ solutions were either a pH of 5 or a concentration of 30%.

The latter affected the flexural strength of the GFRP more severely with a 30% reduction in strength.

Long term immersion in concentrated strong acids will reduce the strength of most FRCs, but iron is dramatically more sensitive. Wastewater environments will have larger concentrations of sulfuric acid present in places where ferrous ions can serve as an energy source for SOB. This explains the rapid corrosion rates in metals and concrete found in wastewater treatment systems and presents the case that polyester composite polymers and other high-grade plastics are resistant to corrosion in this environment because of their inherent lack of iron components or ferrous ions for bacteria to consume or interact with. It is important to note that elements that exist below the water line, or in an otherwise anaerobic environment, are less susceptible to the additional MIC caused by SOB that can yield sulfuric acid. The implication is that iron manhole covers are especially prone to biological corrosion in sewage systems, with most of the damage localized on the bottom surface of the cover and hidden from direct aboveground inspection.

Many studies have been conducted regarding the effect of biocorrosion on iron, steel, aluminum and other metals and alloys, but few have been conducted regarding polymers apart from those that use the corrosion inhibiting properties of polymers to protect metals from corrosion. Therefore, this study fills a gap in the literature by tackling a novel research topic related to the use of manhole covers manufactured from fiber reinforced composites as a viable replacement for current metal manhole covers.

CHAPTER III

METHODOLOGY

This chapter outlines the procedures and equipment utilized to conduct and evaluate the testing used to measure and quantify the effects of chemical exposure on mechanical properties of polyester composites in wastewater service.

It is important to re-iterate that there is no generally agreed upon method to recreate the bacterial environment or microbiologically induced corrosion (MIC) found in wastewater treatment. Neither is there a method to convert hydrogen sulfide vapor concentrations into aqueous sulfuric acid concentrations. The quantities cannot be related chemically using molar mass and a standard chemical equation balance. The effects of the sulfur compound will differ based on the given material, temperature, humidity of the environment, the influence of a biofilm, and other biocorrosion related factors.

For these reasons, the McAllen wastewater treatment plant was chosen as the optimal site to conduct field testing, as the manhole covers nearest to it would be exposed to the uniquely high concentration of sewage, and accordingly, the highest concentration of biologically produced hydrogen sulfide gas.

Table 1: Material Properties for the unsaturated polyester composite samples

Product Description			
Glass fiber reinforced Polyester BMC suitable for manhole covers and other accessories.			
General			
Material Status	Commercial: Active		
Availability	America		
Filler/Reinforcement	Glass Fiber and mineral filler		
Features	Good chemical resistance Excellent stain resistance		
Processing Method	This BMC product is generally intended to be compression molded in matched metal die molds, typically at 300°F (150°C) and 500 to 1000 psi (35-65 BAR) molding pressure. Strength values may be affected by the molding process.		
Resin	Unsaturated Polyester Composite		
Physical	Typical	Unit	Test Method
Specific Gravity	1.73-1.79	-	ASTM D792
Mold Shrinkage	0.0000-0.0022	in/in	ASTM D955
Hardness, Barcol	22-38	Barcol Units	ASTM D2583
Mechanical (D)	Typical	Unit	Test Method
Tensile Strength	4,000 Min	PSI	ASTM D638
Flexural Strength	11,000 Min	PSI	ASTM D790
Impact (D)	Typical	Unit	Test Method
Izod Notched Impact Strength	4.0 Min	ft-Lb/in	ASTM D256

Fiber reinforced composite (FRC) specimens were provided by Composite Access Products (CAP) in the form of coupons and plates, as pictured in Figure 3. The material properties for the unsaturated polyester composite samples are listed in Table 1. Exposure tests were conducted by suspending these specimens above a mass separator where sewage is churned and processed after going through lifting stations and before being sent to grit basins. This is where the highest concentrations of hydrogen sulfide (H₂S) gas and sulfate-reducing

microbiology can be found in a covered wastewater system environment. This is considered a worst-case location for iron-based components in terms of their corrosion risk. In most locations, manhole covers in wastewater collection systems are exposed to less extreme conditions. This area of the plant intentionally uses corrosion resistant materials like stainless steel and coated concrete. The concrete requires protection due to the presence of iron containing compounds, specifically in cement, which can serve as a fertilizer for microbiologically induced corrosion (MIC).

A total of thirty-two 5×0.5×0.125-inch molded polyester FRC coupons were exposed to this environment for periods up to 237 days. Eight square polyester FRC plates of 6×6×0.135-inch were exposed for up to 527 days. Five gray iron tensile bars were exposed for exactly 240 days. The size difference between a molded coupon and a plate is shown in Figure 3. Further information on the specimens and their exposure periods can be found in Table 7 and Table 8 of CHAPTER IV.



Figure 3: Plate and Coupon Sample Size Comparisons

All composite and iron coupons had their weight measured before and after exposure to permit estimation of mass lost using Eq. (1).

$$\text{Corrosion rate} = \frac{\text{Weight loss (g)} \times K}{\text{Material Density} \left(\frac{\text{g}}{\text{cm}^3} \right) \times \text{Exposed Area (cm}^2\text{)} \times \text{Exposure Time (h)}} \quad (1)$$

Many researchers rely on this equation, described in the ASTM G1 standard, to calculate the corrosion rate for metals following corrosive damage, where corrosion rate is in terms of millimeters per year and K serves as a unit conversion factor.

“Considering the mechanisms of polymer corrosion, it is apparent that weight-loss measurements cannot be used to evaluate attack” [21]. This is referencing the statement by Fontana that polymeric materials are attacked by swelling, dissolution, and bond rupture instead of advanced oxidation and wear. However, the mineral fillers in the composite material are potentially sensitive to the environment and may be dissolved by H_2SO_4 so the samples were weighed to verify their integrity.

Suspending both polyester and iron samples in a corrosive environment involved drilling a small hole through each coupon, plate, or bar, and looping them from a vinyl coated clothesline wire, using polymer spacers to keep each sample from contacting neighbors, and varying the length of the spacers to aid in identifying the sequence of the samples in the event of corrosion removing any identifying markers. This arrangement can be seen in Figure 4.



Figure 4: Composite Plates and Iron Bars Suspended in Test Environment

Two C-clamps serve to keep the suspended specimen loop taught and secure. Specimens were attached with redundant dual anchors to help prevent samples or equipment from falling into the sludge below.

Initially, an H₂S sensor with a 400-ppm range was used to gauge the concentration of hydrogen sulfide gas at the field site. It was soon discovered that the H₂S gas concentrations were greater than the instrument range. To remedy this, an OdaLog L2 H₂S gas logger (Model: SL-H2S-2000) was obtained, shown in Figure 5. The gas logger had an operating range of 0 to

2000-ppm and allowed for concentrations to be monitored over the course of a week or longer. It was designed for harsh wastewater environments with a 12-month battery, and data access by Bluetooth™. This device allowed for monitoring the concentrations and temperatures these samples were exposed to during representative periods throughout the year.

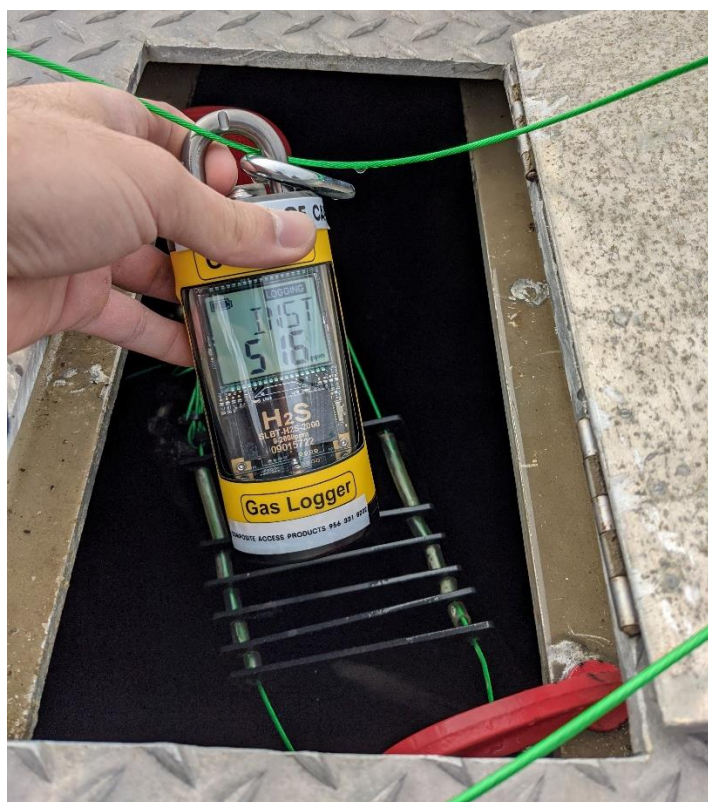


Figure 5: OdaLog L2 Gas Logger

The gas logger was used to measure concentrations for one-week periods during four separate weeks. It was calibrated with a null test after each measurement period. This ensured that concentration measurements did not become offset because of sensor decay due to extended exposure. The pre-use span check calibration was performed at the factory before distribution.

Thirty-two polyester coupons were rotated in and out of the suspension system along with a total of eight polyester plates. The plates were later cut into coupon-sized strips, with the

same width as the thirty-two molded coupons. Each plate yielded 8 to 9 coupons. The resulting specimens, both the standard coupons and plate-derived coupons, were tested using a three-point bending (3PB) test in accordance with ASTM standards D7264 and D7264M. An Instron 5966 material testing system was used along with the appropriate adapters, with a span that was adjusted based on the standards outlined by ASTM and the thickness of the coupons. The test setup can be seen in Figure 6.



Figure 6: Three-Point Bending Test on Instron 5966

Each standalone coupon was tested with a span of 10 cm (3.937 in). Each plate-derived coupon was tested with a span of 11.2 cm (4.409 in), which was in line with the 32:1 support span-to-thickness ratio specification. The coupons were sorted in order of increasing exposure time, and the test results are available in the Appendix.

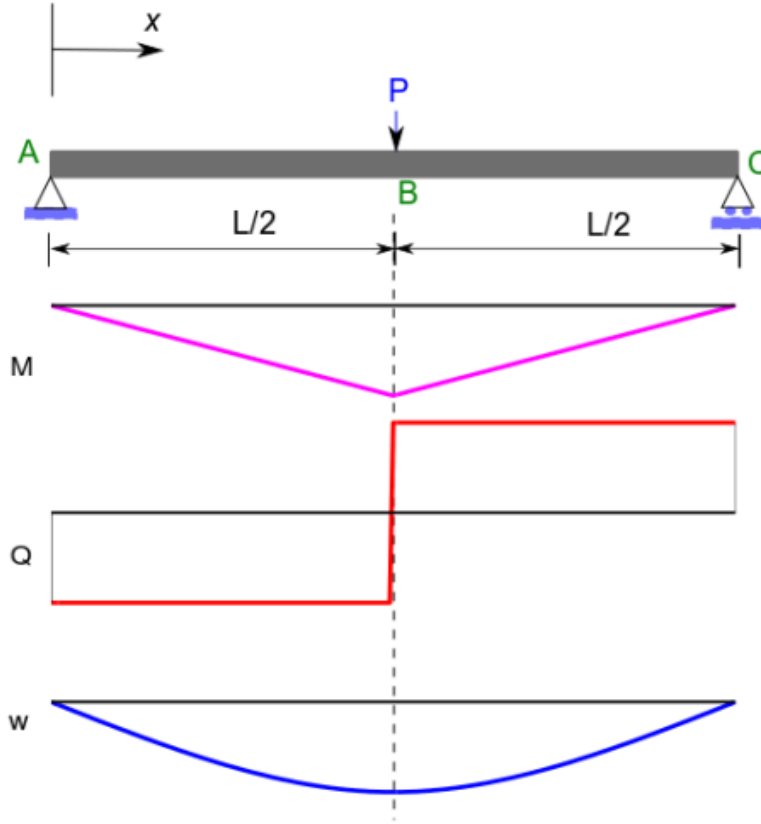


Figure 7: Three-Point Bending Test Schematic and Corresponding Moment (M), Shear (Q), and Deflection (W) graphs [<http://commons.wikimedia.org/wiki/File:SimpSuppBeamPointLoad.svg>]

Most of the comparisons made in this study involve the flexural strength of the material. A three-point bending test was conducted, depicted in Figure 6 – Figure 8, on the beam-shaped FRC specimens. For this test, a beam of length L rests on two roller supports and is subject to a central load P . In these experiments, the length of the beam or coupon that extends past roller supports A and C can be neglected. The Young's modulus is calculated from

$$E = \frac{PL^3}{48\delta I} \quad (2)$$

where δ is defined as the deflection of the beam and I is the second moment of area such that

$$I = \frac{a^3 b}{12} \quad (3)$$

where a denotes the beam's depth or thickness and b describes the beam's width.

Figure 8 gives a closer look at the testing apparatus before the coupon fails.



Figure 8: Coupon in Flexural Stress During Bending Test

In a screening experiment, a single polyester FRC coupon was submerged in undiluted sulfuric acid for 24 hours. The coupon was susceptible to high concentrations of sulfuric acid and swelled as shown in Figure 9.



Figure 9: Swollen Polymer Coupon Matrix

Figure 10 shows a succeeding experiment, where 3 individual sets of 5 coupons were submerged in diluted sulfuric acid solutions with concentrations of 20%, 30%, and 50% by volume. The immersed coupons were sealed and placed inside a fume hood for 14 days at a constant room temperature of 21°C (69°F) before being subjected to flexural tests.



Figure 10: Acid Immersion Tests – Polyester Coupons

The concentrations of the immersion baths shown in Figure 10 and Figure 11 are listed in Table 2. The flexural performance of these coupons is summarized in Table 5 of CHAPTER IV.

Table 2: Concentrations for Immersion Tests

Group	H ₂ SO ₄ [mol/L]	Concentration [%]
Left	3.7	20%
Middle	5.5	30%
Right	9.2	50%

The immersion test or pickle jar test conducted on the FRC coupons was repeated with iron tensile coupons to gauge how iron would respond to acidic attack compared to the FRC material. These coupons were only submerged for 25 hours before distinctive changes were observed.



Figure 11: Acid Immersion Tests - Iron Tensile Coupons

An effort was made to measure the pH of the condensate that tended to form on the suspended samples as an early indicator for the presence of a biofilm forming on the material surface. It was hypothesized that sulfur oxidizing bacteria (SOB) would produce sulfuric acid and lower the pH of any condensate. pH strips were wiped on the surface of the FRC, iron, and the stainless-steel hatch to pick up the condensate. These pH strips can be seen in Figure 12.



Figure 12: pH testing the condensate

A sample group of 4 grey iron tensile bars were exposed to the corrosive field conditions for 8 months and compared against a control group of 4 unexposed grey iron tensile bars. This material is the same material commonly used in manhole covers and is representative of the corrosion effects in the absence of protective films, laminates, or other anti-corrosion treatments. The tensile performance of these samples was evaluated in an Instron electromechanical material testing system (MTS) pictured in Figure 13. The broken specimens are laid out in Figure 14.



Figure 13: Iron Bar Tensile Tests



Figure 14: Iron Tensile Specimens – Exposed for 8 months (Left); Unexposed (Right)

One of the corroded specimens had lost too much material to be properly secured in the MTS and was instead used to measure the expected corrosion rate of the iron samples.

Hardness testing was conducted using a Wilson 574 Series Rockwell Tester shown in Figure 15. Rockwell hardness tests were used to nondestructively analyze the surfaces of the FRC coupons. The HRL scale was utilized, which employs a ball diameter of 6.35 mm (1/4 in) and a major load of 588.4 N (60 kgf). A larger major load would fracture the brittle glass fibers that are not designed to withstand concentrated point loads perpendicular to fiber direction. Hardness testing can be expected to detect loss of filler to acid attack as loss will be greatest near the surface.



Figure 15: HRL Hardness Testing

The 3M Rapid SRB Detection Pouch (Code: 3M-SRB) is a culturing method designed to facilitate field testing by providing fast and accurate results. It allows for a time-based estimate

in terms of colony-forming units per milliliter (CFU/mL) in accordance with the chart in Figure 16.


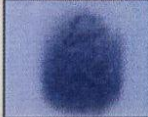

		SRB CFU/mL						
Hours from inoculation to observation		10 ⁶	10 ⁵	10 ⁴	10 ³	10 ²	10 ¹	<10
		8	16	24	32	40	48	62 to 120
		14	22	30	38	46	54	
		22	30	38	46	54	62	
		Day 1	Day 2			Day 3-5		

Figure 16: 3M SRB Detection Pouch Quantitation Estimates

This quantitation chart is based on *D. Desulfuricans* ATCC 29577 and *D. vulgaris* ATCC 29579 which are two standardized SRB species expected in the wastewater environment. A colony-forming unit is a microbiological measurement standard that estimates the amount of bacteria or fungal cells in a sample which are able to multiply via binary fission under controlled conditions. When estimating the number of colonies, it is uncertain if a colony arises from one cell or a group of cells and expressing results in colony-forming units reflects this uncertainty. Incubation instructions follow NACE TM0194-2014 standards, and a sample pouch representative of the wastewater in the field environment can be seen in Figure 17.

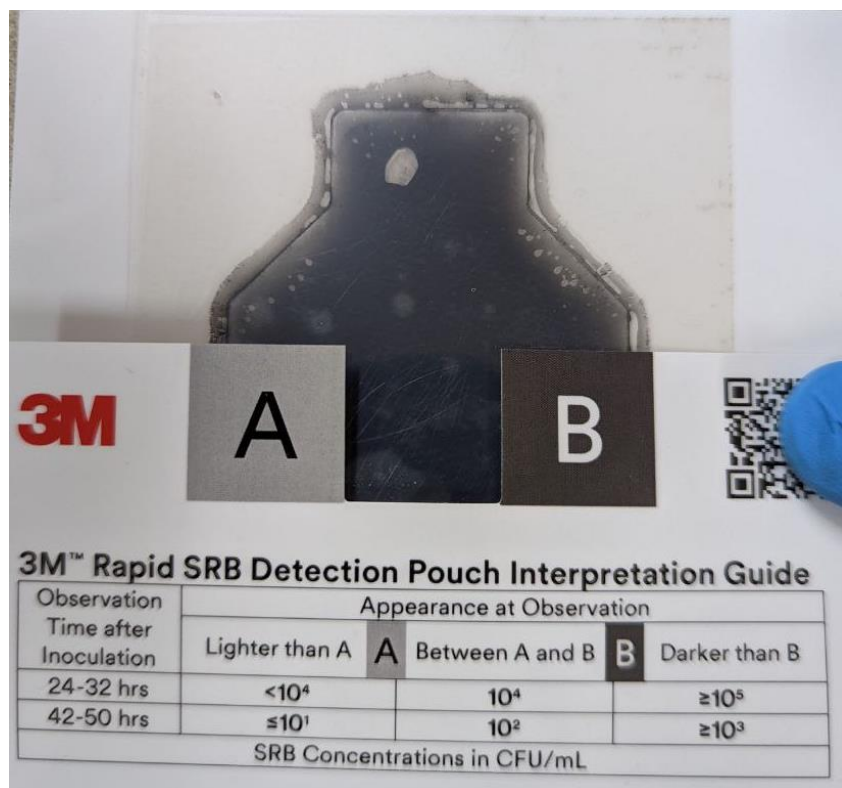


Figure 17: Rapid SRB Detection of water beneath FRC samples

This preliminary detection pouch confirmed the presence of SRB in the water below the suspended coupons with the black coloration forming in just a few minutes on the test media. This means that the concentration of aqueous hydrogen sulfide in the water is greater than 10-ppm and implies an SRB population greater than 10,000,000 CFU/mL which is outside of the effective measurement range for this test.

An FRC plate and an iron slab of equivalent surface area were suspended and tested for the presence of SRB bacteria after a few weeks. These samples were misted with deionized water and scraped with a sterile aluminum tool to extract surface bacteria via a pipette. The images shown in Figure 18 were taken 48 hours after inoculation.

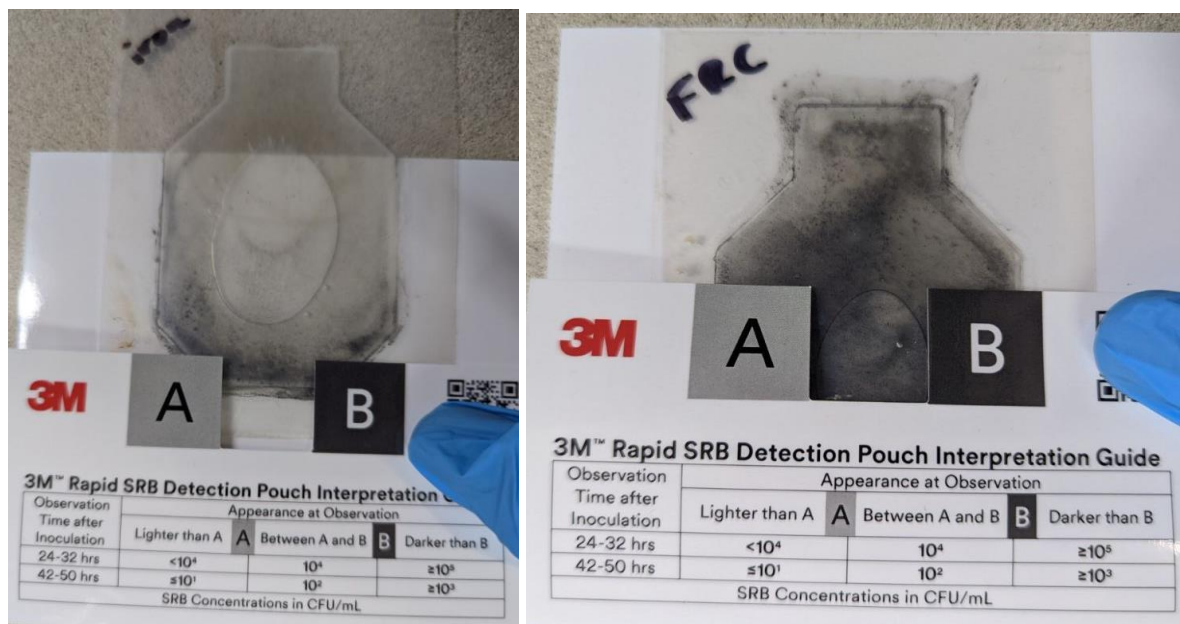


Figure 18: Rapid SRB Detection of Iron Sample (Left), and of Composite Plate (Right)

SRB tend to flourish under the waterline, and it was expected that these tests would show small quantities, if any, of SRB on the suspended samples. The reason iron corrodes so rapidly is suspected to be the formation of a SOB biofilm that uses ferrous ions as an energy source and affects materials with acid attack.

A bacteria broth testing kit from BTS solutions was used to verify this notion. As with the SRB tests, the iron and FRC samples were misted with deionized water and then scraped with a sterile aluminum tool to enable the extraction of any bacteria present on the surface. Here, the moisture was taken from the surface of the materials using a sterile syringe, and then injected into a bacterial broth testing vial, which requires anaerobic conditions. The vials were then placed in an incubating oven set to 28°C.

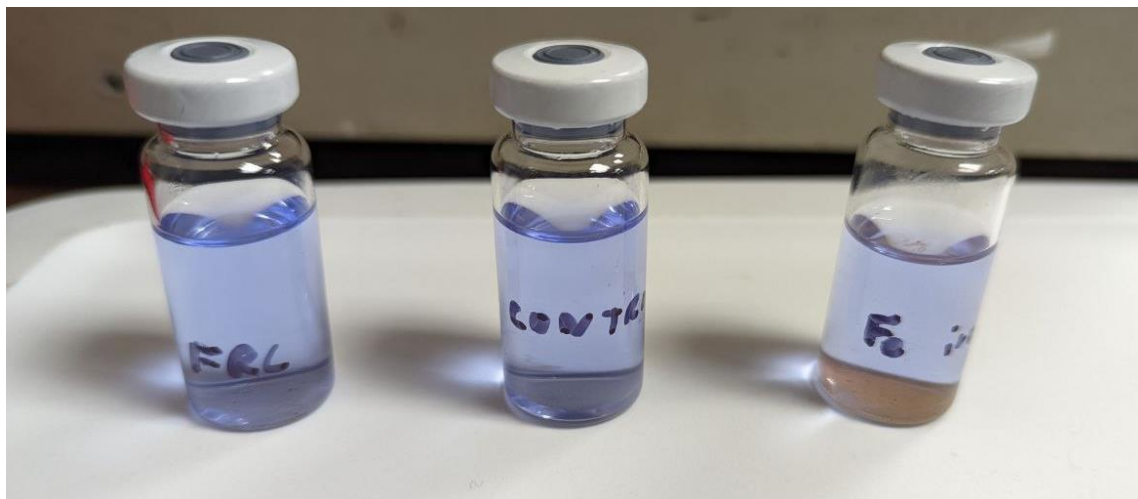


Figure 19: SOB Test Vials – Composite Sample (Left), Control Sample (Middle), and Iron Sample (Right)

These test vials are the more traditional method to test for bacteria colonies in field environments. They contain thiosulfates, inorganic salts, and a pH indicator. The broth is meant to provide the nutrients favorable to SOB growth and will change color over time if SOB bacteria are detected. The weakness of this testing method, that was circumvented by the 3M SRB detection pouches, is the relatively long incubation period required to show results. Also relevant are the total dissolved solids (TDS), which in this case are 0.5% for the bacterial broth. Field samples may have TDS that exceed this quantity and each primary sample has been diluted by two stages to ensure test compatibility.

CHAPTER IV

RESULTS AND ANALYSIS

The OdaLog L2 hydrogen sulfide gas logger continuously measured the concentration and temperature of the environment for seven-day periods. These measurements are presented in Figure 20 – Figure 23. There is an evident leading effect, where a rise in temperature is shortly followed by a rise in hydrogen sulfide concentrations. This is explained by the rise in temperature stimulating bacterial activity, which causes higher rates of gas production.

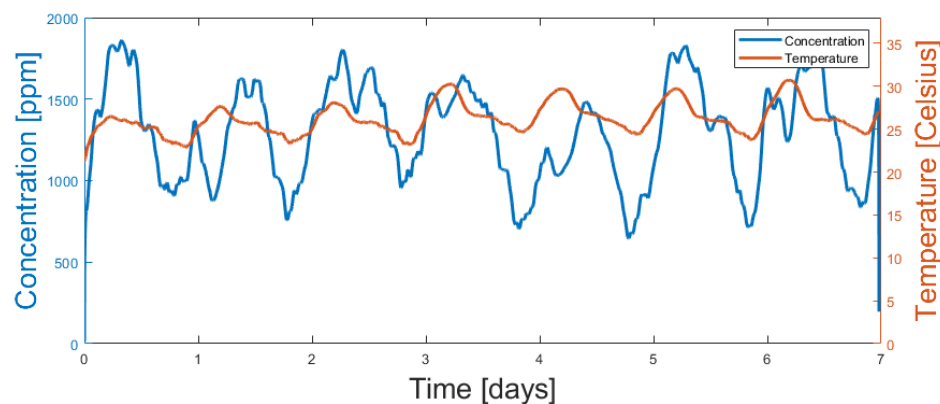


Figure 20: H₂S Concentration and Temperature October 28th to November 4th

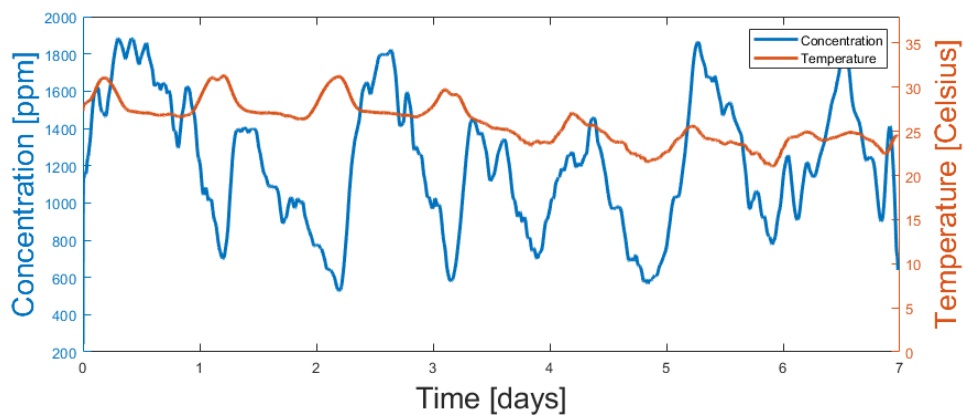


Figure 21: H₂S Concentration and Temperature November 25th to December 2nd

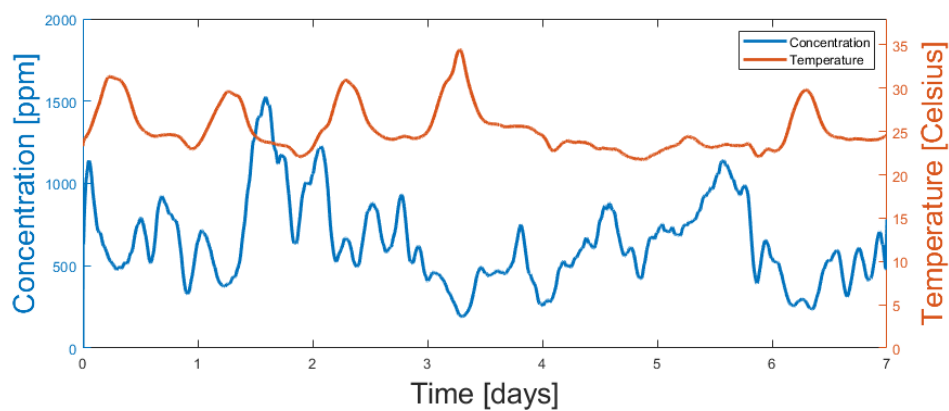


Figure 22: H₂S Concentration and Temperature March 24th to March 31st

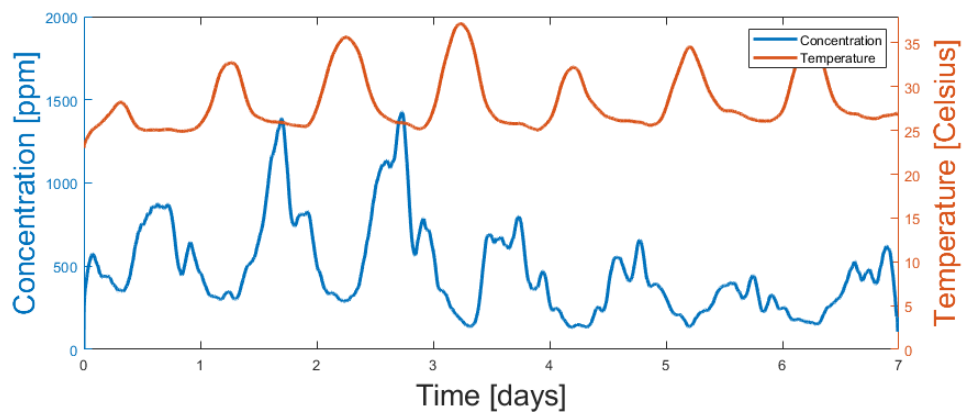


Figure 23: H₂S Concentration and Temperature April 22nd to April 29th

Average concentration values were lower in the spring than in the fall as shown in Table 3. Higher maximum temperatures, shown in Table 4, were observed in the spring, but average concentration values were lower in the spring than in the fall. This shows that average temperatures do not correlate with average concentration values, but other factors, such as the venting cycle of the wastewater treatment plant, may have affected hydrogen sulfide gas production for the bacteria.

Table 3: Concentration Summary for Hydrogen Sulfide Gas Readings

Concentration [ppm]	Oct 2020	Nov 2020	Mar 2021	April 2021
Maximum	1730	1671	1007	885
Minimum	786	680	351	215
Average	1292	1216	646	477

Table 4: Temperature Summary for Hydrogen Sulfide Gas Readings

Temperature [°C]	Oct 2020	Nov 2020	Mar 2021	April 2021
Maximum	30.9	31.6	35.3	37.6
Minimum	21.3	19.6	21.4	23.0
Average	26.2	26.0	25.3	28.2

The laboratory experiment where polyester coupons were immersed in diluted sulfuric acid for 14 days resulted in no visible damage. The flexural results of the specimens are provided in Figure 24 to Figure 26, where flexural stress is compared against flexural strain. The coupons that were exposed to 50 wt% sulfuric acid were showing only slight signs of damage when wiping off residual acid.

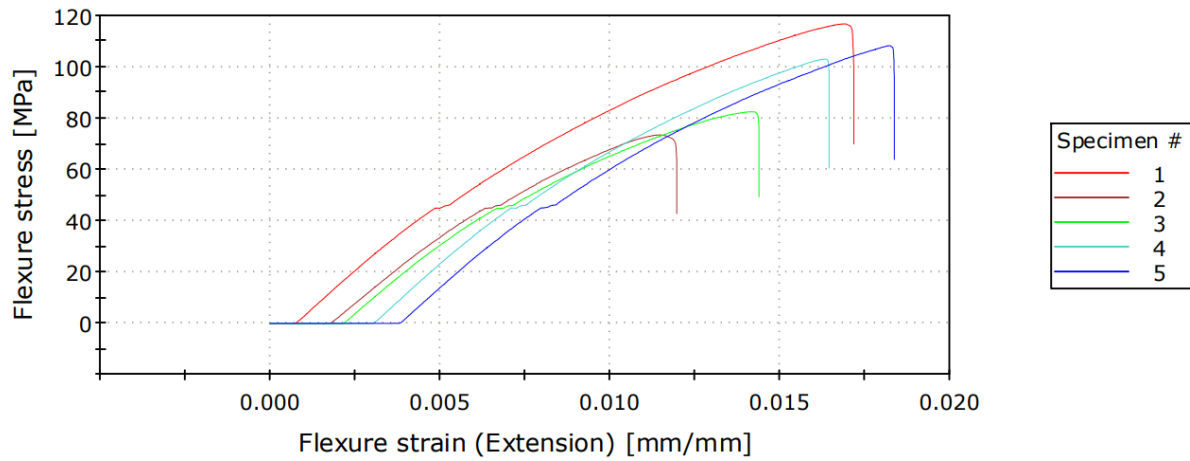


Figure 24: FRC Coupons Exposed to [20 wt%] Sulfuric Acid for 14 days

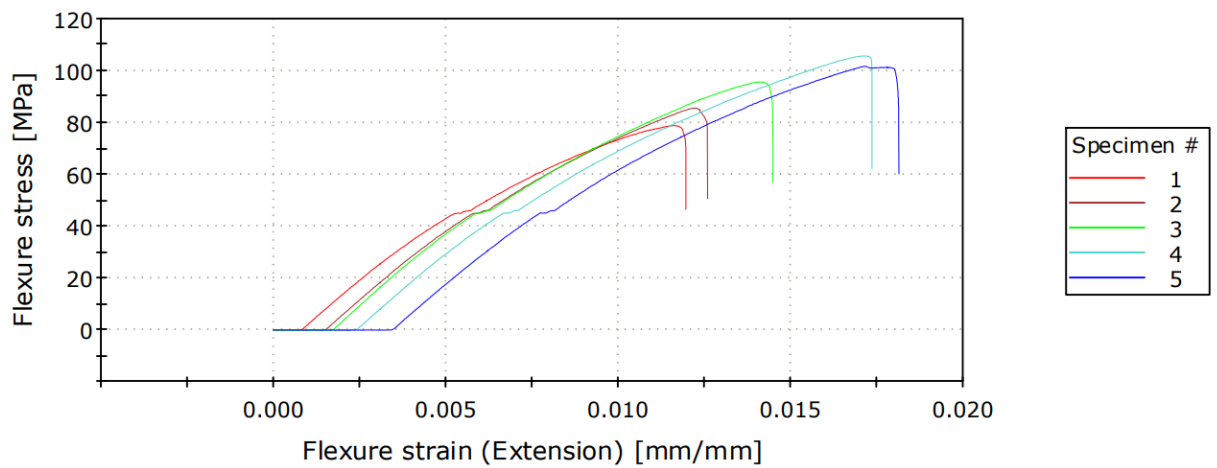


Figure 25: FRC Coupons Exposed to [30 wt%] Sulfuric Acid for 14 days

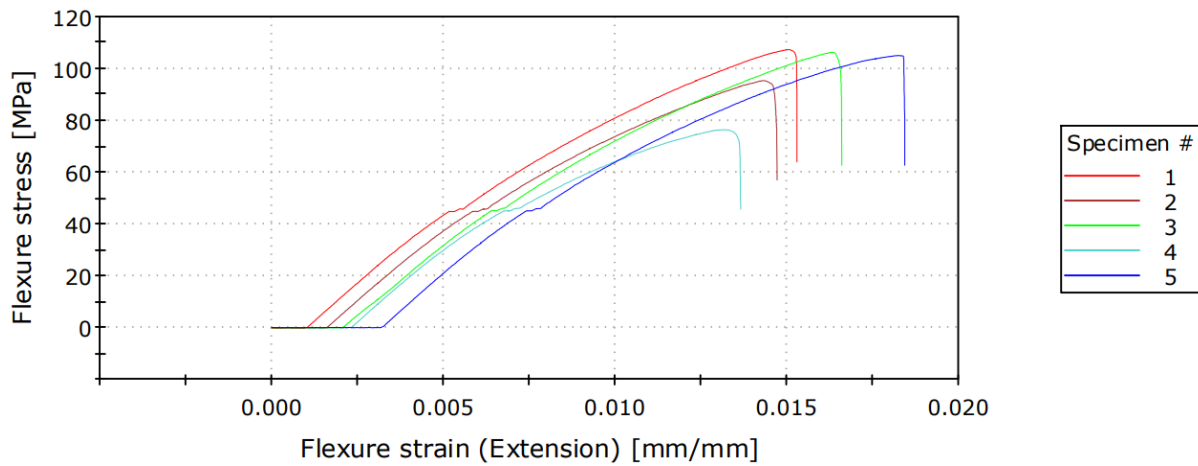


Figure 26: FRC Coupons Exposed to [50 wt%] Sulfuric Acid for 14 days

Table 5 summarizes the flexural results shown in Figure 24 to Figure 26, and lists them in order of increasing sulfuric acid concentration. The values provided were generated by computing the average performance for all the specimens in the same condition set, with an uncertainty value equal to one standard deviation, as is the case for all the tables that summarize flexural results in this section.

Table 5: Average Flexural Test Results of Laboratory Corrosion Conditions

Sulfuric Acid Concentration [wt%]	Young's Modulus [GPa]	Flexural Stress at Break [MPa]	Strain at Break [%]	Energy at Break [J]
0% - Control	12.6 ± 0.5	90.2 ± 18.3	1.35 ± 0.08	0.35 ± 0.06
20%	11.4 ± 0.4	82.1 ± 15.4	1.56 ± 0.25	0.34 ± 0.12
30%	11.4 ± 0.2	77.7 ± 10.7	1.49 ± 0.28	0.32 ± 0.08
50%	11.3 ± 0.3	71.4 ± 17.3	1.57 ± 0.18	0.35 ± 0.08

These results do not show dramatic signs of sulfuric acid attack. Flexural stress at break is the only property that seems to decrease as acid concentration increases, but the wide margin of error makes the results inconclusive. This conclusion is justified by an ANOVA test, which is a statistical tool that can determine if there is disparity or a significant change in the performance of a sample group as compared to other sample groups. This single factor test was conducted with all the flexural data presented in this thesis to verify if certain conditions such as acid concentration or exposure time do indeed weaken the FRC material. Each single factor ANOVA test can only gauge one property at a time, with modulus, flexural stress at break, strain at break, and energy at break each being scrutinized individually. Table 6 contains the ANOVA test for Young's modulus in the laboratory immersion test.

Table 6: ANOVA Test for Young's Modulus in Laboratory Immersion Test

Summary						
Groups	Count	Sum [GPa]	Average [GPa]	Variance [GPa²]	σ [GPa]	
20% H₂SO₄	5	56.9	11.4	0.164	0.404	
30% H₂SO₄	5	57.1	11.4	0.056	0.237	
50% H₂SO₄	5	56.7	11.3	0.084	0.300	
Results						
Source of Variation	SS	df	MS	F	P-value	F _{critical}
Between Groups	0.015	2	0.007	0.07	0.93	3.89
Within Groups	1.214	12	0.101			
Total	1.228	14				

Variance, the square of standard deviation, σ , can be calculated using Eq. (4)

$$Variance = \frac{\sum (X - \bar{x})^2}{n - 1} \quad (4)$$

where n is the number of values in the sample. In the ANOVA results, SS represents sum of squares and df stands for degrees of freedom. Here degrees of freedom between groups is calculated by taking the number of groups and subtracting one. Degrees of freedom within groups is calculated by taking total count and subtracting by the number of groups. Dividing SS by df gives MS , which stands for mean squares. F is the ratio of the MS between groups to the MS within groups. The P -value represents the level of significance. $F_{critical}$ is a value obtained from the statistical F-Distribution table [29] based on the two relevant degrees of freedom.

In these statistical tests, a null hypothesis is proposed that suggests there is not a significant amount of variance between the mean of each group and as such, the values are statistically similar. This hypothesis is confirmed when the P -value in Table 6 is greater than 0.05 and F is less than F_{crit} . Here, these conditions are met, and prove that there is no significant difference between the modulus for any of the specimens that were immersed in sulfuric acid. However, there is a 10% decrease in modulus between the control sample that was

not immersed and the other sample groups that were immersed. This suggests that the sulfuric acid may have weakened the bond between the glass fibers and the surrounding polymer matrix. It should be noted that sulfuric acid baths are not fully representative of the corrosive damage expected in field conditions, but the damage caused by sulfuric acid is similar to the damage experienced by the specimens exposed to field conditions, with the exception that strong acids tend to yield higher corrosion rates. The remaining ANOVA tests for flexural stress at break, strain at break, and energy at break are provided in the Appendix.

To reiterate, eight plates and 32 coupons were exposed to field conditions at the wastewater treatment plant, where unique corrosive conditions are caused by the bacteria that thrive in that environment. The polyester coupons in the sample group shown in the flexural performance graph in Figure 27 were exposed to corrosive conditions for 119 days.

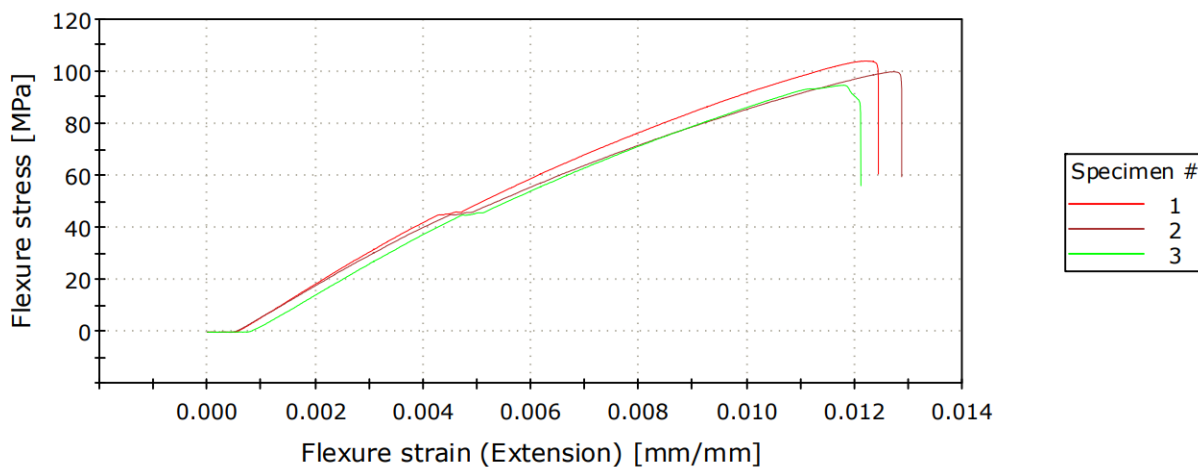


Figure 27: Flexural Test for Coupon Specimens 1 to 3

Figure 27 serves as a representative curve, with the graphical results of the remaining field exposure flexural tests featured in the Appendix. Each sample group is composed of 3 to 4 coupons with field exposure periods ranging between 29 and 237 days. Their flexural performance is summarized in Table 7. The coupons derived from the eight polyester plates were

exposed for periods ranging between 47 and 524 days, and their flexural performance is summarized in Table 8. These tables summarize the Young's modulus, maximum flexural stress, strain at break, and energy at break for each coupon, and are sorted by increasing exposure period. Each of these categories is displayed individually in the graphs presented in Figure 28 through Figure 35.

Table 7: Average Flexural Test Results for All Plate-Derived Coupons

Plate	Exposure [days]	Young's Modulus [GPa]	Flexural Stress at Break [MPa]	Strain at Break [%]	Energy at Break [J]
Control	0	11.5 ± 1.3	52.2 ± 10.3	1.71 ± 0.48	0.47 ± 0.12
1	47	12.3 ± 1.5	63.2 ± 09.6	1.84 ± 0.24	0.52 ± 0.09
3	47	11.3 ± 2.0	45.3 ± 17.1	1.56 ± 0.69	0.41 ± 0.27
2	240	10.9 ± 0.3	50.8 ± 10.9	1.39 ± 0.22	0.38 ± 0.13
5	287	10.9 ± 0.7	81.2 ± 30.1	1.97 ± 0.44	0.77 ± 0.32
6	316	09.9 ± 0.6	61.8 ± 11.1	1.79 ± 0.26	0.54 ± 0.15
7	351	12.0 ± 0.8	63.8 ± 15.4	1.60 ± 0.09	0.54 ± 0.14
4	367	11.3 ± 0.3	49.8 ± 25.8	1.36 ± 0.42	0.38 ± 0.25
8	524	11.0 ± 1.1	51.1 ± 05.4	1.49 ± 0.19	0.39 ± 0.11

Table 8: Average Flexural Test Results for All Coupons

Polyester Coupons	Exposure [days]	Young's Modulus [GPa]	Flexural Stress at Break [MPa]	Strain at Break [%]	Energy at Break [J]
Control	0	12.6 ± 0.5	90.2 ± 18.3	1.35 ± 0.08	0.35 ± 0.06
13,14,15,16	29	12.8 ± 0.3	102.7 ± 9.6	1.40 ± 0.11	0.38 ± 0.05
17,18,19,20	64	12.5 ± 0.3	80.9 ± 24.4	1.27 ± 0.15	0.32 ± 0.08
21,22,23,24	92	12.3 ± 0.1	80.1 ± 8.9	1.19 ± 0.08	0.28 ± 0.03
1,2,3	119	12.3 ± 0.4	90.7 ± 7.4	1.25 ± 0.04	0.30 ± 0.02
25,26,27,28	127	12.4 ± 0.4	99.1 ± 9.0	1.37 ± 0.15	0.37 ± 0.08
4,5,6	148	12.6 ± 0.3	84.4 ± 13.7	1.35 ± 0.13	0.34 ± 0.05
7,8,9	183	12.6 ± 0.5	76.6 ± 16.0	1.28 ± 0.14	0.32 ± 0.07
10,11,12	211	12.5 ± 0.4	74.5 ± 11.6	1.15 ± 0.11	0.27 ± 0.04
29,30,31,32	237	13.1 ± 0.3	97.6 ± 9.2	1.38 ± 0.17	0.36 ± 0.09

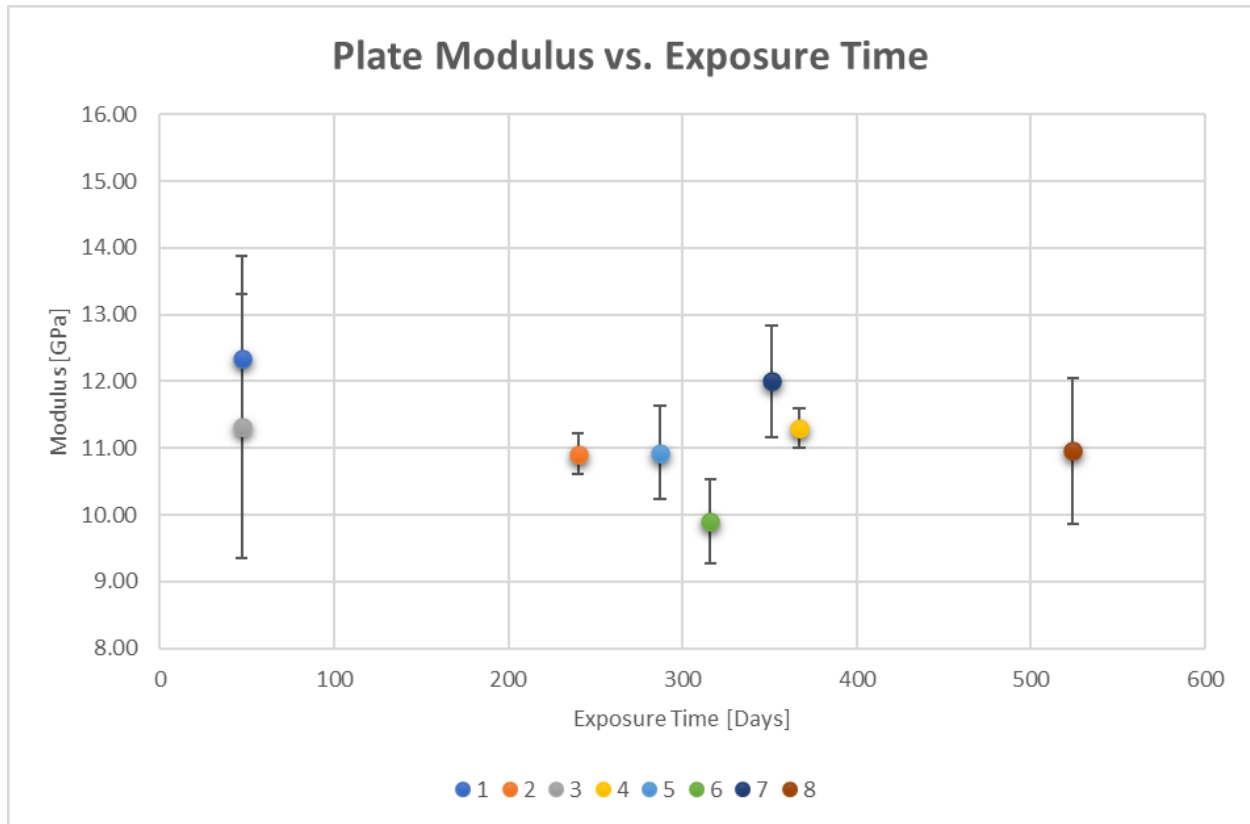


Figure 28: Field Testing - Plate Young's Modulus versus Exposure Time

Table 9: ANOVA Test for Plate Young's Modulus in Field Test

Summary								
Groups	Count	Sum [GPa]	Average [GPa]	Variance [GPa²]	σ [GPa]			
Plate 1	4	49.4	12.3	2.35	1.53			
Plate 2	3	32.7	10.9	0.09	0.30			
Plate 3	3	34.0	11.3	3.91	1.98			
Plate 4	3	33.9	11.3	0.08	0.29			
Plate 5	3	32.8	10.9	0.49	0.70			
Plate 6	3	29.7	9.9	0.40	0.63			
Plate 7	3	36.0	12.0	0.70	0.84			
Plate 8	4	43.8	11.0	1.20	1.09			
Results								
Source of Variation			SS	df	MS	F	P-value	Fcritical
Between Groups			12.969	7	1.853	1.52	0.22	2.58
Within Groups			21.987	18	1.222			
Total			34.957	25				

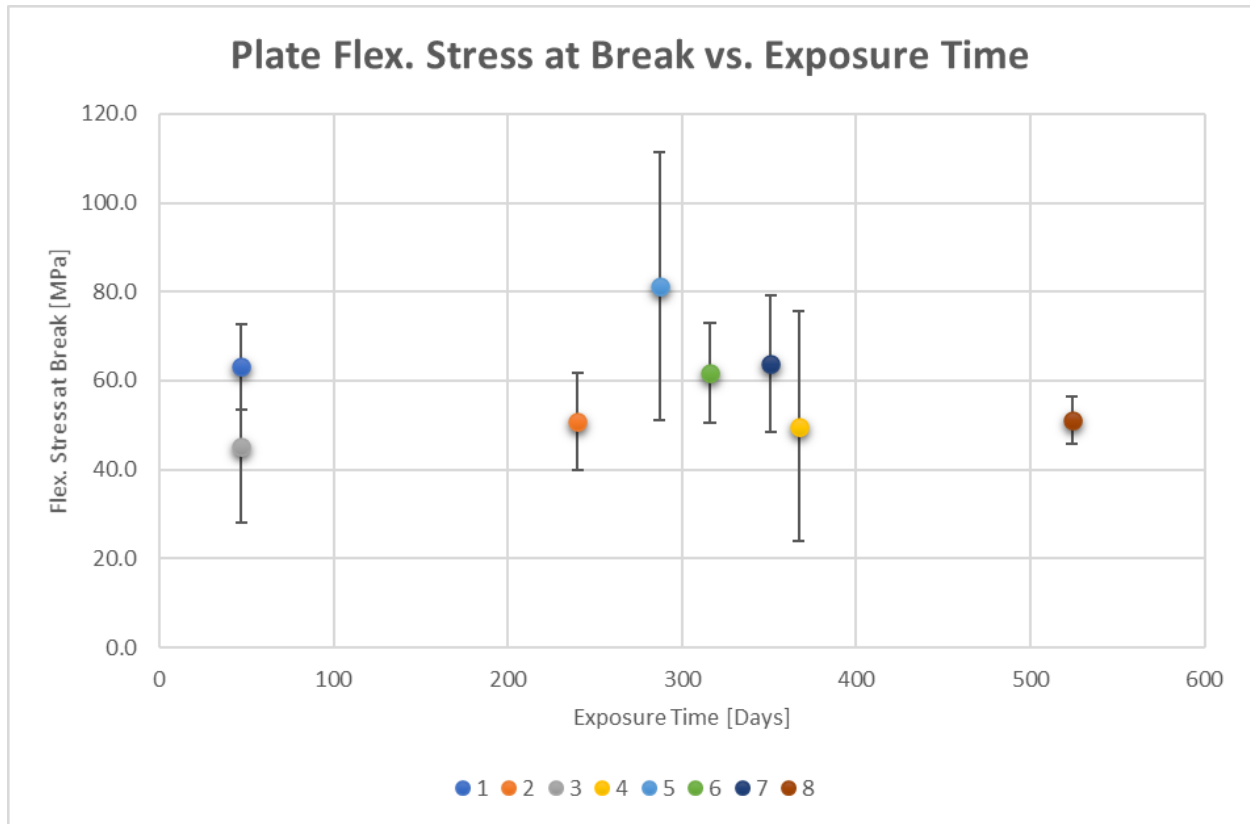


Figure 29: Field Testing - Plate Flexural Stress at Break versus Exposure Time

Table 10: ANOVA Test for Plate Flexural Stress at Break in Field Test

Summary								
Groups	Count	Sum [MPa]	Average [MPa]	Variance [MPa²]	σ [MPa]			
Plate 1	4	252.7	63.2	92.7	9.6			
Plate 2	3	152.4	50.8	118.7	10.9			
Plate 3	3	135.9	45.3	293.7	17.1			
Plate 4	3	149.2	49.7	666.7	25.8			
Plate 5	3	243.6	81.2	906.4	30.1			
Plate 6	3	185.3	61.8	123.7	11.1			
Plate 7	3	191.4	63.8	236.7	15.4			
Plate 8	4	204.4	51.1	29.2	5.4			
Results								
Source of Variation			SS	df	MS	F	P-value	Fcritical
Between Groups			2898.8	7	414.1	1.47	0.24	2.58
Within Groups			5057.7	18	281.0			
Total			7956.5	25				

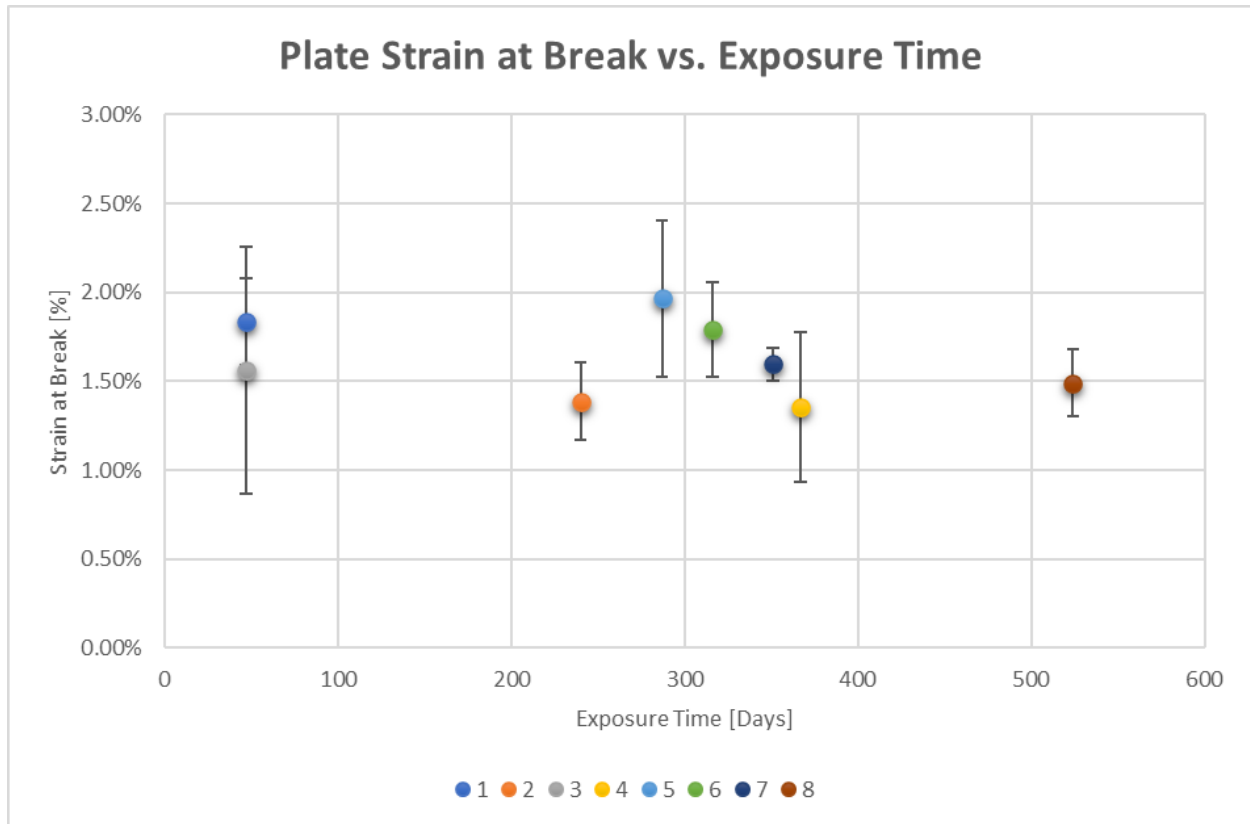


Figure 30: Field Testing - Plate Strain at Break versus Exposure Time

Table 11: ANOVA Test for Plate Strain at Break in Field Test

Summary							
Groups	Count	Sum [%]	Average [%]	Variance [%²]	σ [%]		
Plate 1	4	7.35E-02	1.84E-02	5.93E-06	2.44E-03		
Plate 2	3	4.16E-02	1.39E-02	4.80E-06	2.19E-03		
Plate 3	3	4.69E-02	1.56E-02	4.80E-05	6.93E-03		
Plate 4	3	4.07E-02	1.36E-02	1.76E-05	4.19E-03		
Plate 5	3	5.90E-02	1.97E-02	1.92E-05	4.38E-03		
Plate 6	3	5.37E-02	1.79E-02	6.92E-06	2.63E-03		
Plate 7	3	4.79E-02	1.60E-02	8.93E-07	9.45E-04		
Plate 8	4	5.96E-02	1.49E-02	3.62E-06	1.90E-03		
Results							
Source of Variation		SS	df	MS	F	P-value	Fcritical
Between Groups		1.09E-04	7	1.56E-05	1.25	0.33	2.58
Within Groups		2.24E-04	18	1.24E-05			
Total		3.32E-04	25				

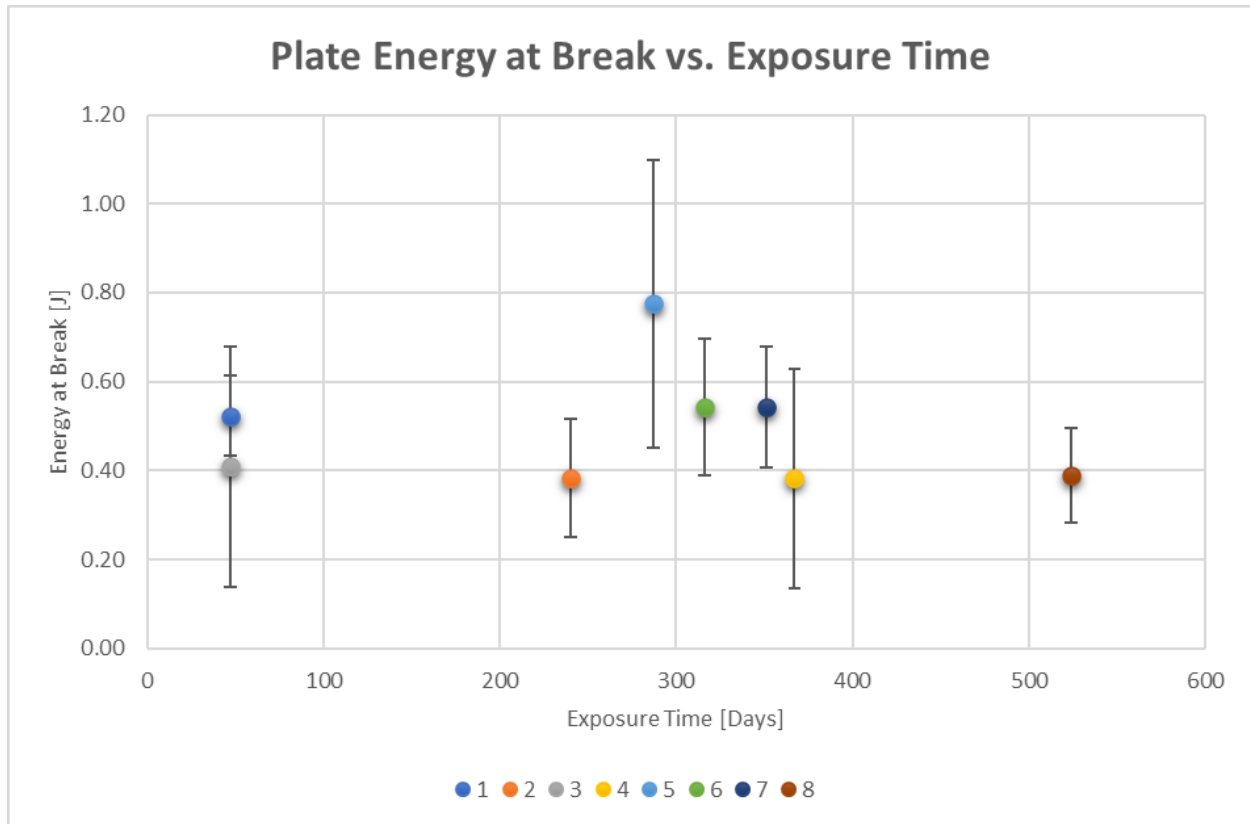


Figure 31: Field Testing - Plate Energy at Break versus Exposure Time

Table 12: ANOVA Test for Plate Energy at Break in Field Test

Summary								
Groups	Count	Sum [J]	Average [J]	Variance [J²]	σ [J]			
Plate 1	4	2.09	0.52	0.01	0.09			
Plate 2	3	1.15	0.38	0.02	0.13			
Plate 3	3	1.23	0.41	0.07	0.27			
Plate 4	3	1.15	0.38	0.06	0.25			
Plate 5	3	2.32	0.77	0.10	0.32			
Plate 6	3	1.62	0.54	0.02	0.15			
Plate 7	3	1.63	0.54	0.02	0.14			
Plate 8	4	1.56	0.39	0.01	0.11			
Results								
Source of Variation			SS	df	MS	F	P-value	Fcritical
Between Groups			0.39	7	0.06	1.54	0.22	2.58
Within Groups			0.65	18	0.04			
Total			1.05	25				

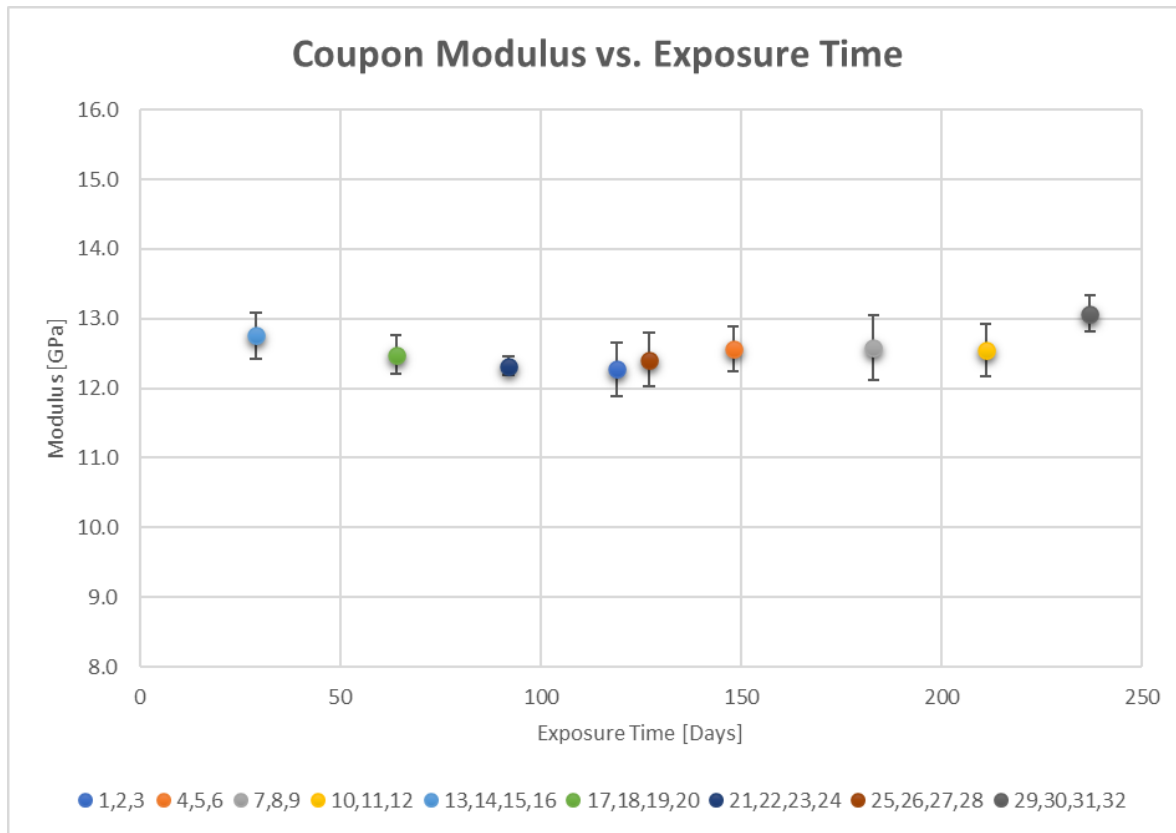


Figure 32: Field Testing - Coupon Young's Modulus versus Exposure Time

Table 13: ANOVA Test for Coupon Young's Modulus in Field Test

Summary							
Coupon Groups	Count	Sum [GPa]	Average [GPa]	Variance [GPa²]	σ [GPa]		
1,2,3	3	36.8	12.3	0.15	0.39		
4,5,6	3	37.7	12.6	0.10	0.32		
7,8,9	3	37.8	12.6	0.21	0.46		
10,11,12	3	37.6	12.5	0.14	0.38		
13,14,15,16	4	51.0	12.8	0.11	0.33		
17,18,19,20	4	49.9	12.5	0.08	0.28		
21,22,23,24	4	49.3	12.3	0.02	0.14		
25,26,27,28	4	49.6	12.4	0.15	0.38		
29,30,31,32	4	52.3	13.1	0.07	0.27		
Results							
Source of Variation		SS	df	MS	F	P-value	Fcritical
Between Groups		1.808	8	0.226	2.08	0.08	2.37
Within Groups		2.503	23	0.109			
Total		4.311	31				

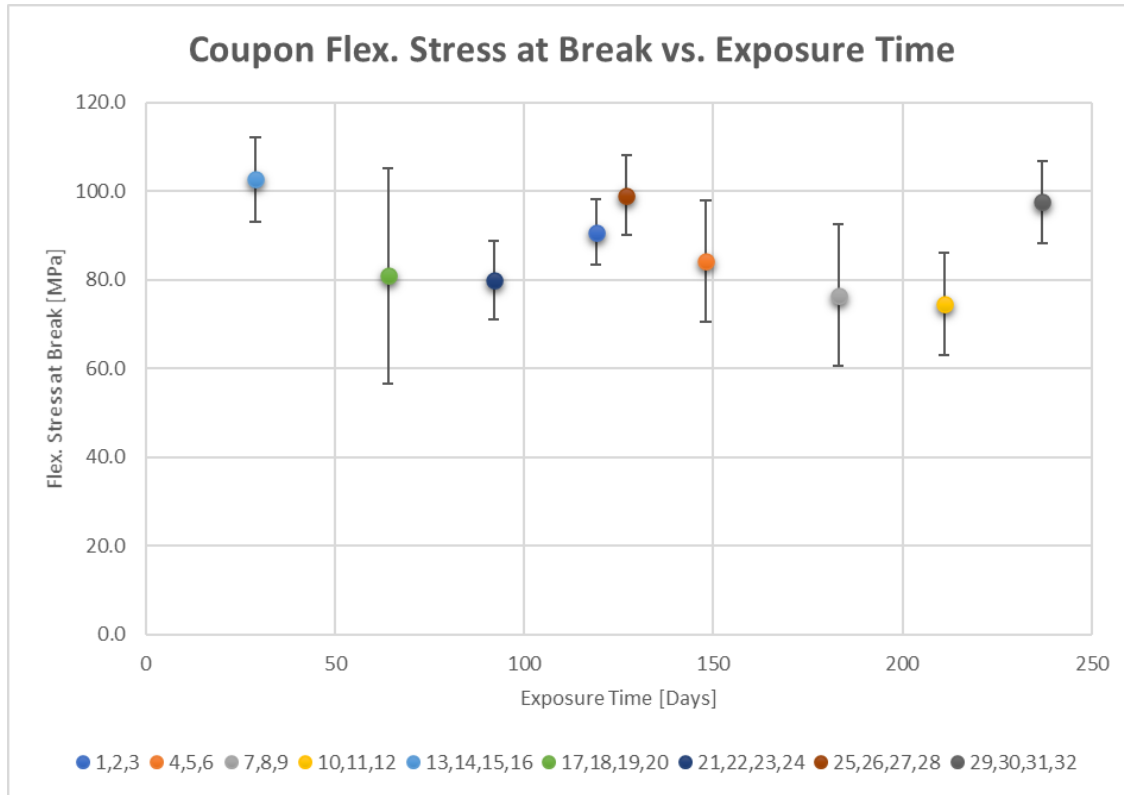


Figure 33: Field Testing - Coupon Flexural Stress at Break versus Exposure Time

Table 14: ANOVA Test for Coupon Flexural Stress at Break in Field Test

Summary							
Coupon Groups	Count	Sum [MPa]	Average [MPa]	Variance [MPa ²]	σ [MPa]		
1,2,3	3	272.2	90.7	54.5	7.4		
4,5,6	3	253.0	84.3	187.3	13.7		
7,8,9	3	229.8	76.6	254.6	16.0		
10,11,12	3	223.5	74.5	134.1	11.6		
13,14,15,16	4	410.7	102.7	92.8	9.6		
17,18,19,20	4	323.6	80.9	594.7	24.4		
21,22,23,24	4	320.2	80.0	78.8	8.9		
25,26,27,28	4	396.4	99.1	80.9	9.0		
29,30,31,32	4	390.4	97.6	84.8	9.2		
Results							
Source of Variation		SS	df	MS	F	P-value	F _{critical}
Between Groups		3175.0	8	396.9	2.25	0.06	2.37
Within Groups		4056.7	23	176.4			
Total		7231.7	31				

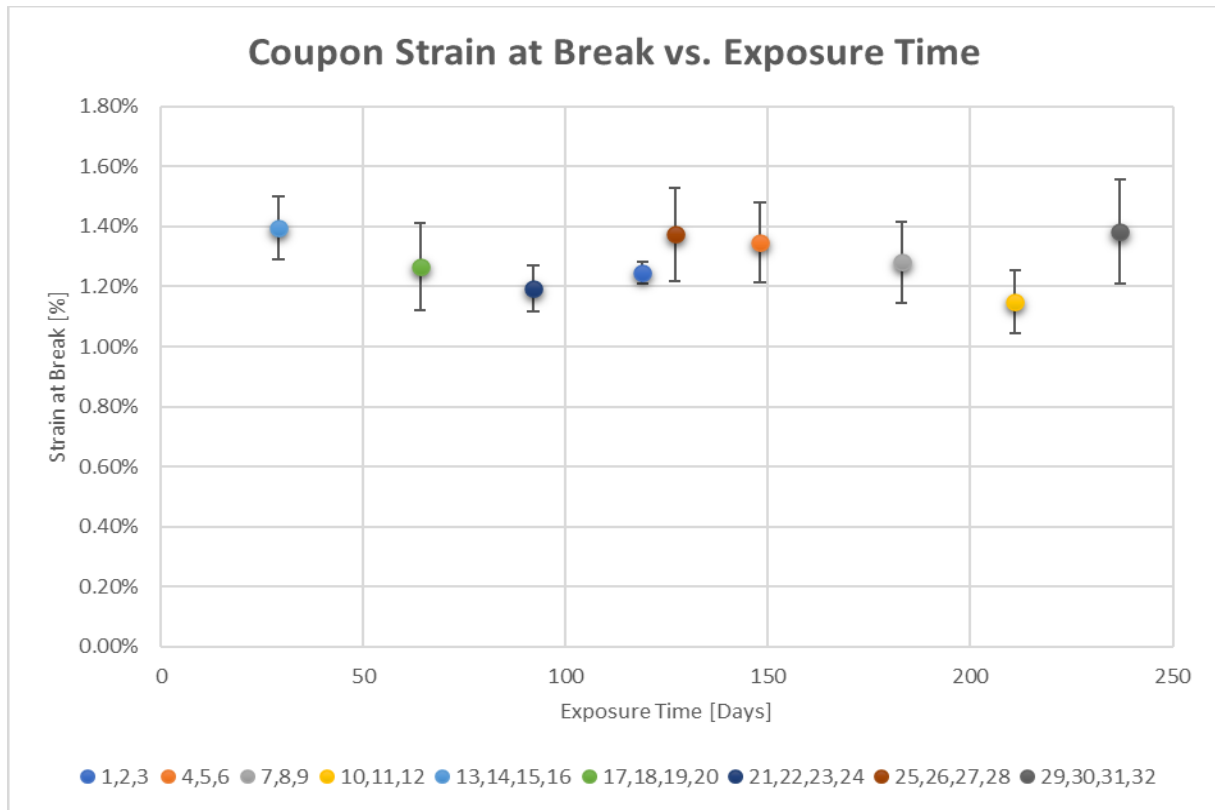


Figure 34: Field Testing - Coupon Strain at Break versus Exposure Time

Table 15: ANOVA Test for Coupon Strain at Break in Field Test

Summary							
Coupon Groups	Count	Sum [%]	Average [%]	Variance [%²]	σ [%]		
1,2,3	3	3.74E-02	1.25E-02	1.46E-07	3.82E-04		
4,5,6	3	4.04E-02	1.35E-02	1.80E-06	1.34E-03		
7,8,9	3	3.84E-02	1.28E-02	1.87E-06	1.37E-03		
10,11,12	3	3.45E-02	1.15E-02	1.11E-06	1.05E-03		
13,14,15,16	4	5.58E-02	1.40E-02	1.11E-06	1.05E-03		
17,18,19,20	4	5.06E-02	1.27E-02	2.13E-06	1.46E-03		
21,22,23,24	4	4.77E-02	1.19E-02	6.09E-07	7.80E-04		
25,26,27,28	4	5.49E-02	1.37E-02	2.37E-06	1.54E-03		
29,30,31,32	4	5.53E-02	1.38E-02	3.05E-06	1.75E-03		
Results							
Source of Variation		SS	df	MS	F	P-value	Fcritical
Between Groups		2.20E-05	8	2.75E-06	1.68	0.16	2.37
Within Groups		3.77E-05	23	1.64E-06			
Total		5.97E-05	31				

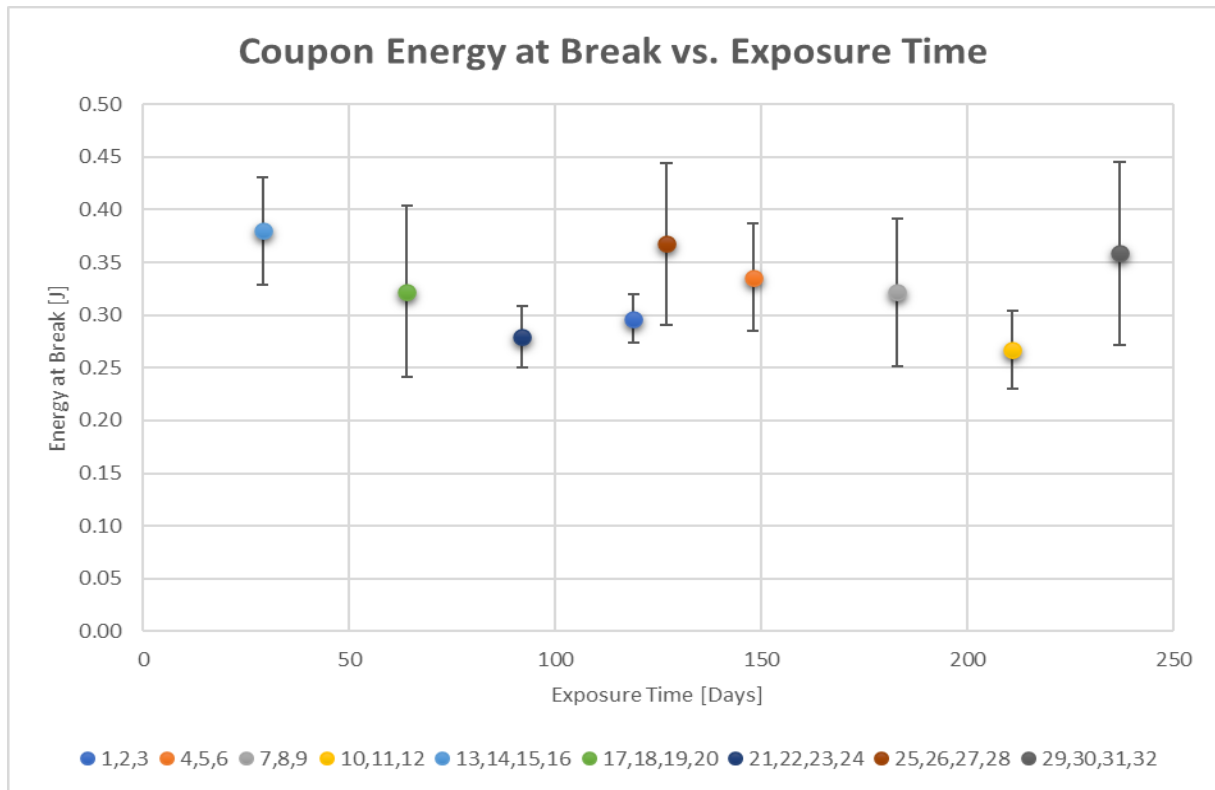


Figure 35: Field Testing - Coupon Energy at Break versus Exposure Time

Table 16: ANOVA Test for Coupon Energy at Break in Field Test

Summary							
Coupon Groups	Count	Sum [J]	Average [J]	Variance [J²]	σ [J]		
1,2,3	3	0.89	0.30	5.20E-04	0.02		
4,5,6	3	1.01	0.34	2.62E-03	0.05		
7,8,9	3	0.96	0.32	4.88E-03	0.07		
10,11,12	3	0.80	0.27	1.35E-03	0.04		
13,14,15,16	4	1.52	0.38	2.60E-03	0.05		
17,18,19,20	4	1.29	0.32	6.54E-03	0.08		
21,22,23,24	4	1.12	0.28	8.39E-04	0.03		
25,26,27,28	4	1.47	0.37	5.82E-03	0.08		
29,30,31,32	4	1.43	0.36	7.56E-03	0.09		
Results							
Source of Variation		SS	df	MS	F	P-value	F _{critical}
Between Groups		4.46E-02	8	5.57E-03	1.44	0.23	2.37
Within Groups		8.88E-02	23	3.86E-03			
Total		1.33E-01	31				

Table 9 through Table 16 contain the ANOVA test results for all the coupons and plate-derived coupons that were exposed to the wastewater environment field conditions throughout this study. As previously stated, when discussing laboratory tests, a *P-value* greater than 0.05, and an F value less than $F_{critical}$ will confirm the null hypothesis that there is not a significant statistical deviation between groups. These conditions are met in every single ANOVA test, which prove statistically that there is no measurable decline in strength in the polyester FRC material because of exposure to the wastewater environment. Figure 32 and Figure 33 are outliers in that the Young's modulus and stress at break properties only marginally passed this statistical test, as shown by a low P-value in Table 13 and Table 14. This would carry more significance if it were not for the sample set with the longest exposure period having some of the best performance in both cases.

The composite coupon samples had their weights measured before and after field exposure with the intent of measuring corrosion via mass loss. All samples had a starting and ending weight within 1% of each other which could be attributed to measurement error or a buildup of residue over time. Five iron samples were suspended for 240 days to serve as a point of comparison. The composite samples had no visible signs of corrosion (no pitting, discoloration, or significant change in mass), whereas the iron samples were crumbling and flaking apart as previously evidenced in Figure 14. The composite samples were rinsed to remove mineral deposits or residue before measuring. Their start and end weights, summarized in Table 17, were all within 1.2%, with an average weight gain of $0.11 \pm 0.37\%$. This was ascribed to leftover mineral deposits, as the hardness tests summarized in Table 18 do not show evidence of swelling or water absorption.

Table 17: Changes in Coupon Mass after Exposure

Polyester Coupon	Original Weight [g]	Ending Weight [g]	Change in Mass [%]
1	8.89	9.00	1.18%
2	8.84	8.94	1.08%
3	8.90	8.97	0.77%
4	8.89	8.89	0.00%
5	8.97	8.97	0.00%
6	8.90	8.90	0.04%
7	8.90	8.90	-0.01%
8	8.92	8.92	-0.04%
9	8.88	8.88	0.02%
10	8.89	8.90	0.08%
11	8.93	8.93	0.04%
12	8.95	8.96	0.11%
13	8.76	8.76	0.01%
14	8.81	8.81	0.00%
15	8.79	8.79	0.00%
16	8.85	8.75	-1.13%
17	8.76	8.76	0.01%
18	8.80	8.80	0.03%
19	8.78	8.77	-0.06%
20	8.80	8.80	0.00%
21	8.80	8.81	0.08%
22	8.80	8.81	0.10%
23	8.80	8.81	0.10%
24	8.80	8.81	0.08%
25	8.75	8.77	0.19%
26	8.83	8.84	0.15%
27	8.80	8.81	0.09%
28	8.77	8.78	0.08%
29	8.73	8.76	0.32%
30	8.80	8.81	0.10%
31	8.86	8.87	0.12%
32	8.87	8.88	0.10%

Table 18: Rockwell Hardness Tests for FRC Coupons Exposed to Field Conditions

Polyester Coupons	Exposure [Days]	Hardness [HRL]
Control	0	90.6 \pm 1.2
13,14,15,16	29	92.1 \pm 1.4
17,18,19,20	64	90.8 \pm 1.6
21,22,23,24	92	91.6 \pm 2.6
1,2,3	119	91.5 \pm 1.7
25,26,27,28	127	91.9 \pm 2.8
4,5,6	148	92.1 \pm 2.5
7,8,9	183	93.0 \pm 1.1
10,11,12	211	92.5 \pm 0.9
29,30,31,32	237	93.0 \pm 2.5

The iron tensile specimens that were exposed to wastewater conditions for 240 days as a base of comparison have their tensile results summarized in Table 19. The peak stress exhibited by the specimens were compared to the average strength of the unexposed iron control samples, with the table showing their change in strength as a percentage. The discrepancy in strength for the three iron specimens can be explained by their arrangement in Figure 4. A few of the specimens may have been in contact, which doubles the effective surface area that acts as a food source for the sulfur oxidizing bacteria (SOB) that feed on ferrous ions. Some specimens were also shielded from the sludge splashing from below by the neighboring fiber reinforced composite (FRC) plates. These circumstantial conditions may have caused some iron tensile bars to be better preserved than others.

Table 19: Gray Iron Tensile Test Results

Name	Peak Stress [ksi]	Avg. Change in Strength [%]
Control 1	36.7	
Control 2	37.5	
Control 3	38.0	
Control 4	39.7	
Specimen 1	26.5	-30.3%
Specimen 2	22.7	-40.2%
Specimen 3	20.0	-47.5%

The relative corrosion rate of the fourth iron tensile specimen was calculated using the values listed in Table 20. The calculated corrosion rate is 0.67 mm/y (26.4 mils per year). To obtain a standard for comparison, a set of experimental corrosion rates were borrowed from Odio *et al.* [28], which show the rates for corrosive wear when exposing mild steel to different environmental conditions. The cast iron tensile specimens are electrochemically similar to mild steel and perform comparatively on the galvanic series. The corrosion rate experienced in the wastewater treatment plant is far more accelerated than those found in other natural environments and compares more closely to immersion in a strong acid like hydrochloric acid.

Table 20: Properties Used to Calculate Corrosion Rate for Iron Tensile Specimen

Property	Value
Starting Weight [g]	110.5
Ending Weight [g]	92.4
Material Density [g/cm ³]	7.15
Surface Area [cm ²]	57.3
Exposure Time [Hours]	5760

Table 21: Experimental Corrosion Rates for Mild Steel [28]

Media	Corrosion Rate [mm/y]
HCl	2.556
Soil	0.017
Atmosphere	0.009
Salt Water	0.060
Fresh Water	0.014

The 3M rapid sulfate reducing bacteria (SRB) detection tests yielded the concentration results shown in Table 22. These results are displayed in [CFU/ml] where CFU is defined as colony forming units. According to the quantitation estimate chart provided in Figure 16, and after an inoculation period of 48 hours at room temperature of 22°C (72°F), the sample derived from iron had bacterial amounts equivalent to 10 CFU/ml, while the composite coupon had bacterial amounts equivalent to 100 CFU/ml. SRB is expected to thrive below the water level, as exhibited by the wastewater sample. It was expected to find trace amounts of SRB on the iron and FRC samples because of the aerotolerant property of the bacteria. SRB does not contribute directly to the deterioration of materials, but the hydrogen sulfide gas that it produces is one of the food sources for SOB bacteria which are the main degrading component.

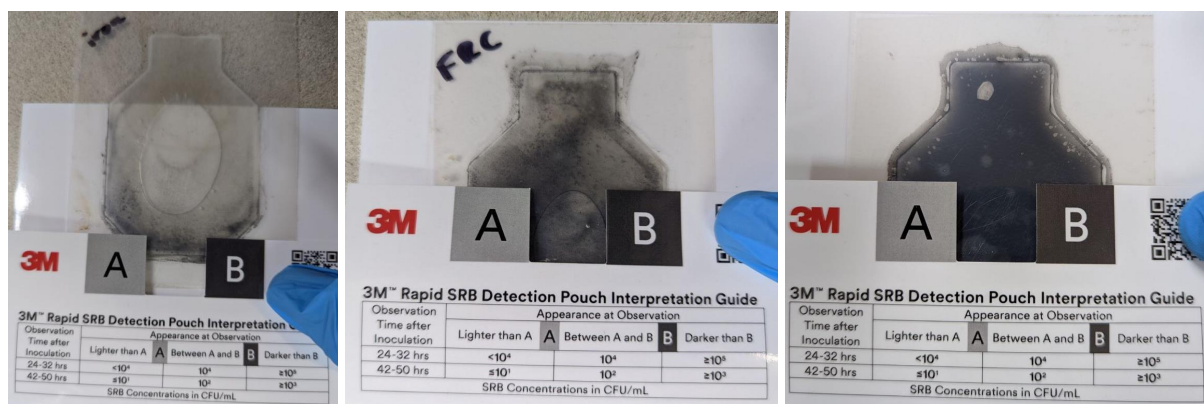


Figure 36: 3M Rapid SRB Tests for Iron (Left), FRC (Middle), Wastewater (Right)

Table 22: SRB Concentrations for Varying Mediums

Sample	SRB Concentration [CFU/mL]
Iron	10
Wastewater	>100,000,000
FRC	100

After two weeks of incubation in a temperature-controlled environment of 28°C (82.4°F), the SOB bacterial broths began forming salt precipitates. These were present in all the incubated vials but were more present in the undiluted FRC, and undiluted iron vials. Salt precipitates are one of the requirements for the test to be valid. The second requirement is a color change which is why the FRC and iron samples are compared against the control sample in Figure 37. A positive result, shown in the iron sample, confirms the presence of excessive SOB bacteria over

the FRC sample, and confirms the hypothesis that SOB bacteria are causing corrosive damage to iron in wastewater environments.

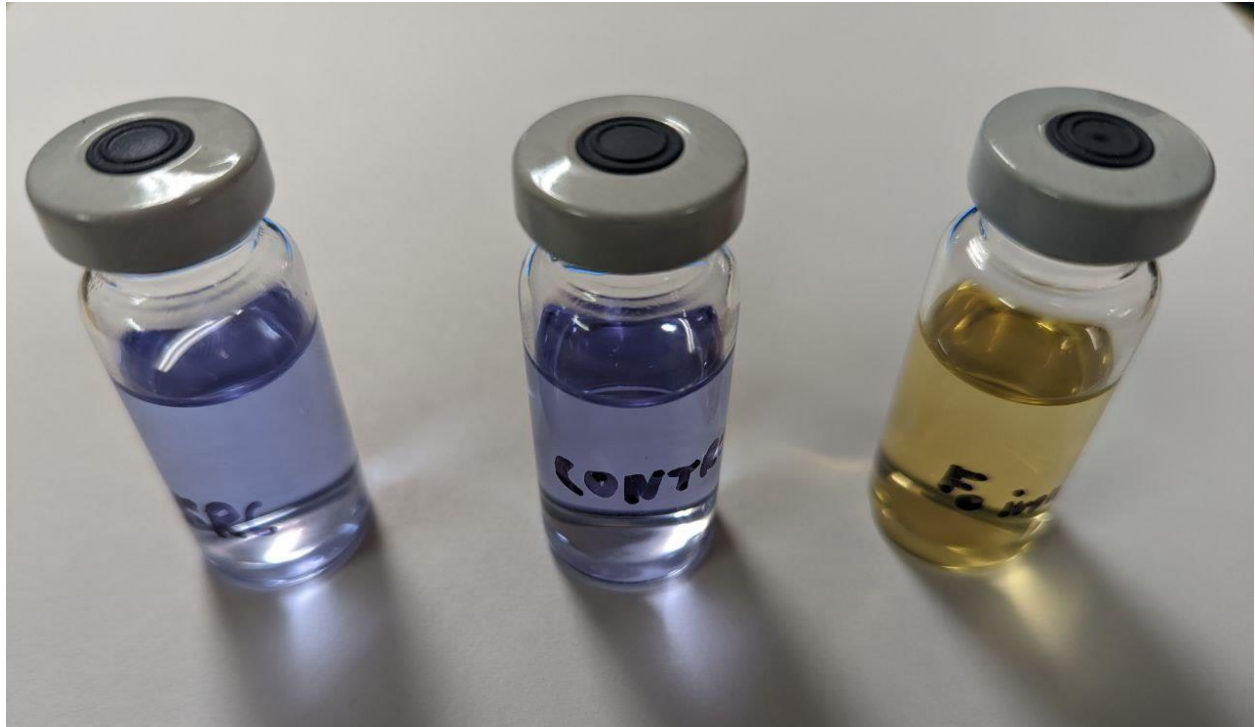


Figure 37: SOB Bacteria Test Results: FRC (Left), Control (Middle), Iron (Right)

CHAPTER V

CONCLUSIONS AND FUTURE WORK

This study was conducted to gauge the effectiveness of a polyester fiber reinforced composite (FRC) material for use in manhole covers near wastewater conditions or sewage drains where microbiologically induced corrosion (MIC) is a present threat. The FRC material is exposed to a wastewater treatment plant in field exposure tests, and is submerged in sulfuric acid on some laboratory tests. It is then subjected to hardness tests, mass change tests, and flexural tests to determine if there is a reduction in strength after up to 524 days of exposure to a wastewater treatment plant, where one of the greatest sources of MIC can be found. Gray iron tensile bars were also tested to serve as a direct comparison to the FRC material.

The strength of this polyester FRC material is not compromised in wastewater service as proven by the flexural tests and supporting statistical analyses. This is more a measure of the integrity of the polymer matrix, which has anti-corrosion properties that prevented any corrosive wear at the surface level of the material. The other components of the composite may be more prone to corrosive damage.

The highly corrosive environment is uniquely caused by bacterial activity, which is difficult to replicate externally. The sulfur oxidizing bacteria (SOB) that thrives in a sewage environment is largely responsible for the advanced oxidation and corrosion present in ferrous materials. Bacteria like *Acidithiobacillus Ferrooxidans* use ferrous ions as an energy source,

accelerating the rate of oxidation in some metals, while also producing a thin film of sulfuric acid which compounds the corrosive effect.

The natural corrosion resistance of the polyester FRC material, coupled with its lack of ferrous ions for bacteria to consume, explains its unaffected strength in the corrosive wastewater environment. The longest exposure period for a given specimen was 524 days. Further testing would require exposure periods that surpass this number, as there is no guarantee that the strength of the FRC would remain completely unaffected throughout its service life. Cyclic loading, like that experienced by a manhole cover in service, could expose some of the filler and fibers of the composite material alongside microcracks. A future experiment would couple cyclic loading with corrosion exposure or cut the composite to expose a larger internal surface area to corrosion. This would determine if the corrosion resistance exhibited here is an intrinsic property of the composite or if it is only derived from the protection provided by the surrounding polymer matrix. This would also answer whether a filler that becomes exposed after cyclic loading would be a point of vulnerability for the material, as the calcium carbonate filler should readily react with acids, confirming whether substituting an iron-based filler is an option, or if it would only expose the material to SOB attack.

There is evidence of localized corrosion downwind of the wastewater plant where this study was conducted. It was long believed that hydrogen sulfide gas was highly corrosive, but after emerging from the exposure area, the gas logger does not register hydrogen sulfide gas concentrations greater than 1 ppm more than a few feet away from the testing site. It is likely that airborne bacteria are latching onto ferrous surfaces and forming SOB colonies that are rapidly advancing the corrosion of nearby metals.

Another point of interest is comparing several iron and FRC samples directly to prove the capability of the material over its traditional corrosion-prone counterpart. This would involve introducing equal amounts of iron and FRC specimens to the environment and rotating out specimens on an established schedule. This would grant insight into the anticipated life expectancy of gray iron in terms of its strength and show when iron loses enough structural integrity to pose a threat to the safety of pedestrians or workers. Side-by-side comparisons of both materials over the course of a few years would further justify replacing gray iron manhole covers with the corrosion resistant FRC material.

Examining some wastewater samples in a microscope would allow for the identification of the specific bacteria involved in MIC, especially if exposing some iron filings to the sample. Watching the bacteria break down iron over time in a microscope would prove that MIC is responsible for the accelerated corrosion rates of iron, and it would determine which bacteria specifically are involved in the process. This would allow for preventative measures that could target the specific species and would confirm which bacteria is responsible for the advanced corrosion rates.

REFERENCES

- [1] Environmental Protection Agency. (n.d.). Municipal Wastewater. EPA. Retrieved April 10, 2022, from <https://www.epa.gov/npdes/municipal-wastewater>.
- [2] J.W. Costerton, K.J. Cheng, G.G. Geesey, T.I. Ladd, J.C. Nickel, M. Dasgupta, T.J. Marrie, Bacterial biofilms in nature and disease, *Annu. Rev. Microbiol.* 41 (1987) 435-464.
- [3] W.A. Hamilton, Sulphate reducing bacteria and anaerobic corrosion, *Annu. Rev. Microbiol.* 39 (1985) 195-217.
- [4] B.J. Little, J.S. Lee, *Microbiologically Influenced Corrosion*, John Wiley & Sons, Inc., 2007.
- [5] F. Bowlus, A. Banta, Control of anaerobic decomposition in sewage transportation, *Water Works Sewerage* 79 (1932) 369.
- [6] Wu, M., Wang, T., Wu, K., & Kan, L. (2020). Microbiologically induced corrosion of concrete in sewer structures: A review of the mechanisms and phenomena. *Construction and Building Materials*, 239, 117813.
- [7] Japan Sewage Works Agency, Corrosion control measures for sewerage structure: Technologies for corrosion prevention and protection, 2007.
https://www.jswa.go.jp/e/r_d/r_d2/pdf/009.pdf, (accessed 10 April 2022).
- [8] R.F. Mueller, W.G. Characklis, W.L. Jones, J.T. Sears, Characterization of initial events in bacterial surface colonization by two *Pseudomonas* species using image analysis, *Biotechnol. Bioeng.* 39 (1992) 1161-1170
- [9] Y.H. An, R.J. Friedman, Concise review of mechanisms of bacterial adhesion to biomaterial surfaces, *J. Biomed. Mater. Res.* 43 (1998) 228-348.
- [10] M.A. Javed, P.R. Stoddart, S.L. McArthur, S.A. Wade, The effect of metal microstructure on the initial attachment of *Escherichia coli* to 1010 carbon steel, *Biofouling* 29 (2013) 939-952.
- [11] M.A. Javed, P.R. Stoddart, E.A. Palombo, S.L. McArthur, S.A. Wade, Inhibition or acceleration: bacterial test media can determine the course of microbiologically influenced corrosion, *Corros. Sci.* 86 (2014) 149-158.
- [12] W.M. Dunne Jr., Bacterial adhesion: seen any good biofilms lately?, *Clin Microbiol. Rev.* 15 (2002) 155-166.
- [13] I.B. Beech, C.C. Gaylarde, Attachment of *Pseudomonas fluorescens* and *Desulfovibrio desulfuricans* to mild and stainless steel – first step in biofilm formation, in: C.A.C.

- Sequeira (Ed.), Microbial corrosion, European federation of corrosion publications, Proceedings of the 2nd International EFC Workshop; 1991 March 3-6; Sesimbra (Portugal), pp. 61-66.
- [14] G. Bradley, C.C. Gaylarde, Iron uptake by *Desulfovibrio vulgaris* outer membrane components in artificial vesicles, *Curr. Microbiol.* 17 (1988) 189-192.
 - [15] I.B. Beech, C.C. Gaylarde, Adhesion of *Desulfovibrio desulfuricans* and *Pseudomonas fluorescens* to mild steel surfaces, *J. Appl. Bacteriol.* 67 (1989) 201-207.
 - [16] R.A. King, J.D.A. Miller, D.S. Wakerley, Corrosion of mild steel in cultures of sulphate reducing bacteria: effect of changing the soluble iron concentration during growth, *Br. Corros. J.* 8 (1973) 89-93.
 - [17] R.A. King, C.K. Dittmer, J.D.A. Miller, Effect of ferrous ion concentration on the corrosion of iron in semicontinuous cultures of sulphate-reducing bacteria, *Br. Corros. J.* 11 (1976) 105-107.
 - [18] Vuković, M., Pesic, B., Štrbac, N., Mihajlović, I., & Sokić, M. (2012). Linear polarization study of the corrosion of iron in the presence of *Thiobacillus ferrooxidans* bacteria. *International Journal of Electrochemical Science*, 7(3), 2487-2503.
 - [19] W. K. Choi, Electrochemical Aspects of Metal Sulfide Bioleaching and Biocorrosion (Ph. D. diss.), New Mexico Institute of Mining and Technology, Socorro, (1990).
 - [20] B. K. Little and P. A. Wagner, An Electrochemical Evaluation of Microbiologically Induced Corrosion by Two Iron-oxidizing Bacteria, *CORROSION/86*, (1986).
 - [21] Fontana, M. G., & Greene, N. D. (2018). Corrosion engineering. McGraw-hill.
 - [22] Witsman YH (1991) Fatigue of Composite Materials. Elsevier, New York
 - [23] Adams RD, Singh MM (1996) They dynamic properties of fiber-reinforced polymers exposed to hot, wet conditions. *Compos Sci Technol* 56(8):977.
 - [24] Kumar BG, Singh RP, Nakamura T (2002) Degradation of carbon fiber reinforced epoxy composites by ultraviolet radiation and condensation. *J Compos Mater* 36(24):2713.
 - [25] Nakamura, T., Singh, R. P., & Vaddadi, P. (2006). Effects of environmental degradation on flexural failure strength of fiber reinforced composites. *Experimental mechanics*, 46(2), 257-268.
 - [26] Feng, P., Wang, J., Wang, Y., Loughery, D., & Niu, D. (2014). Effects of corrosive environments on properties of pultruded GFRP plates. *Composites Part B: Engineering*, 67, 427-433.

- [27] Yahagi, Y., & Mizutani, Y. (1987). Corrosive wear of cast iron in sulphuric acid.
- [28] Odio, B. O., Chinwuko, E. C., Chukwuneke, J. L., & Sinebe, J. E. (2014). Investigation of the effect of corrosion on mild steel in five different environments. *Int. J. Sci. Technol. Res*, 3, 306-310.
- [29] Illowsky, B., Holmes, A., Dean, S. (2018). *Introductory Business Statistics*. Hong Kong: Samurai Media Limited.

APPENDIX

APPENDIX

ADDITIONAL SUBJECT MATERIALS

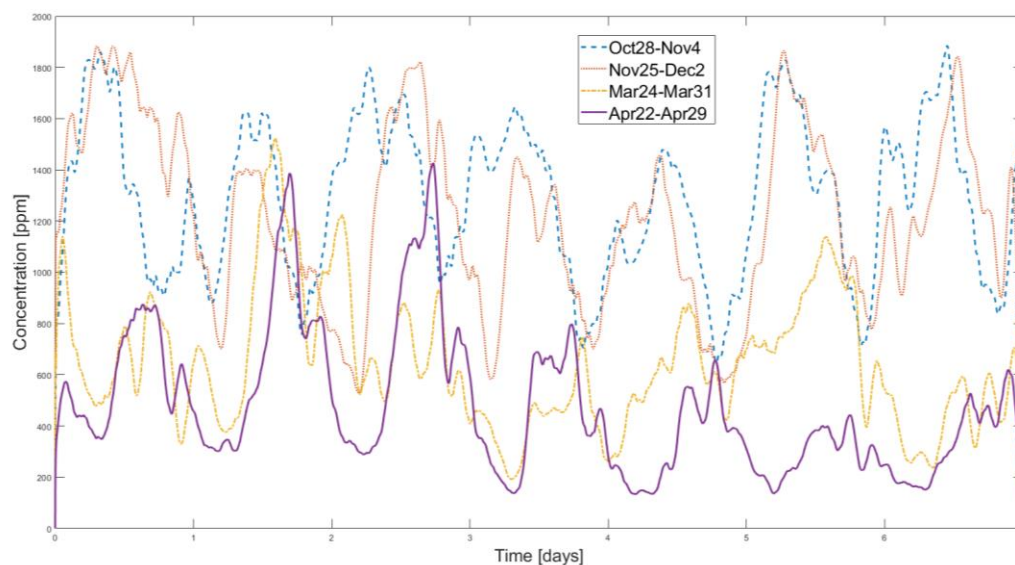


Figure 38: Gas Logger H₂S Data in Test Site – overlaid

Table 23: ANOVA Immersion Test Flexural Stress

Summary								
Groups	Count	Sum [MPa]	Average [MPa]	Variance [MPa ²]		σ [MPa]		
20% H ₂ SO ₄	5	410.3	82.1	238.6		15.4		
30% H ₂ SO ₄	5	388.4	77.7	114.3		10.7		
50% H ₂ SO ₄	5	357.1	71.4	300.9		17.3		
Results								
Source of Variation			SS	df	MS	F	P-value	F _{critical}
Between Groups			285.6	2	142.8	0.66	0.54	3.89
Within Groups			2615.0	12	217.9			
Total			2900.7	14				

Table 24: ANOVA Immersion Test Flexural Strain

Summary							
Groups	Count	Sum [%]	Average [%]	Variance [%²]	σ [%]		
20% H₂SO₄	5	7.82E-02	1.56E-02	6.36E-06	2.52E-03		
30% H₂SO₄	5	7.44E-02	1.49E-02	7.64E-06	2.76E-03		
50% H₂SO₄	5	7.86E-02	1.57E-02	3.38E-06	1.84E-03		
Results							
Source of Variation		SS	df	MS	F	P-value	Fcritical
Between Groups		2.15E-06	2	1.07E-06	0.19	0.83	3.89
Within Groups		6.96E-05	12	5.80E-06			
Total		7.17E-05	14				

Table 25: ANOVA Immersion Test Energy at Break

Summary							
Groups	Count	Sum [J]	Average [J]	Variance [J²]	σ [J]		
20% H₂SO₄	5	1.72	0.34	1.39E-02	0.12		
30% H₂SO₄	5	1.60	0.32	6.91E-03	0.08		
50% H₂SO₄	5	1.77	0.35	5.71E-03	0.08		
Results							
Source of Variation		SS	df	MS	F	P-value	Fcritical
Between Groups		3.15E-03	2	1.57E-03	0.18	0.84	3.89
Within Groups		1.06E-01	12	8.84E-03			
Total		1.09E-01	14				

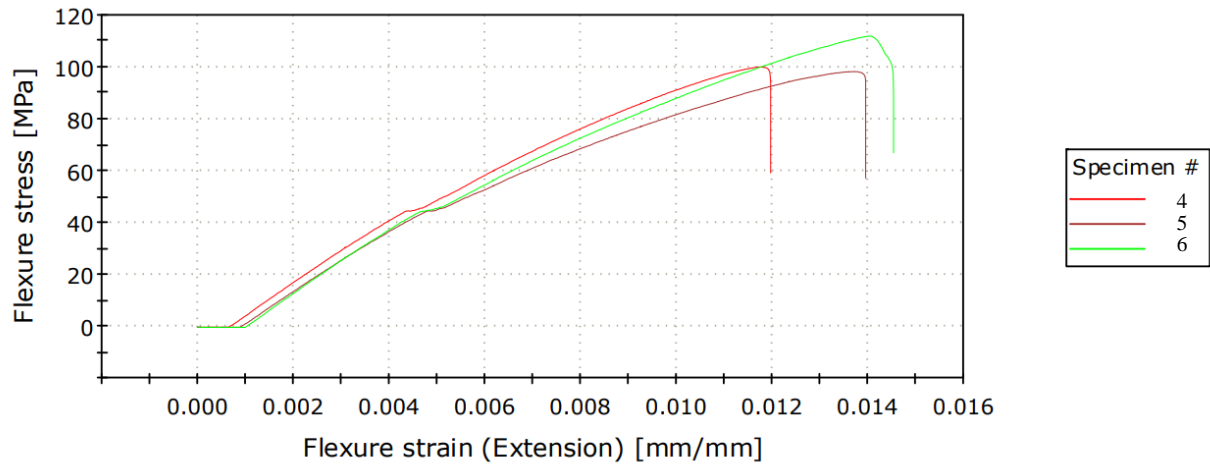


Figure 39: Flexural Tests for Coupons 4 to 6

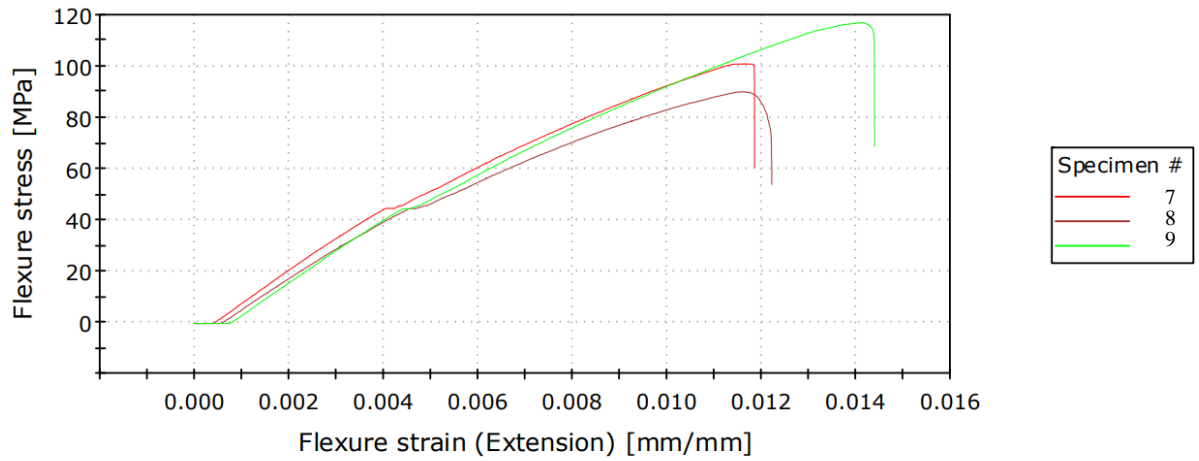


Figure 40: Flexural Tests for Coupons 7 to 9

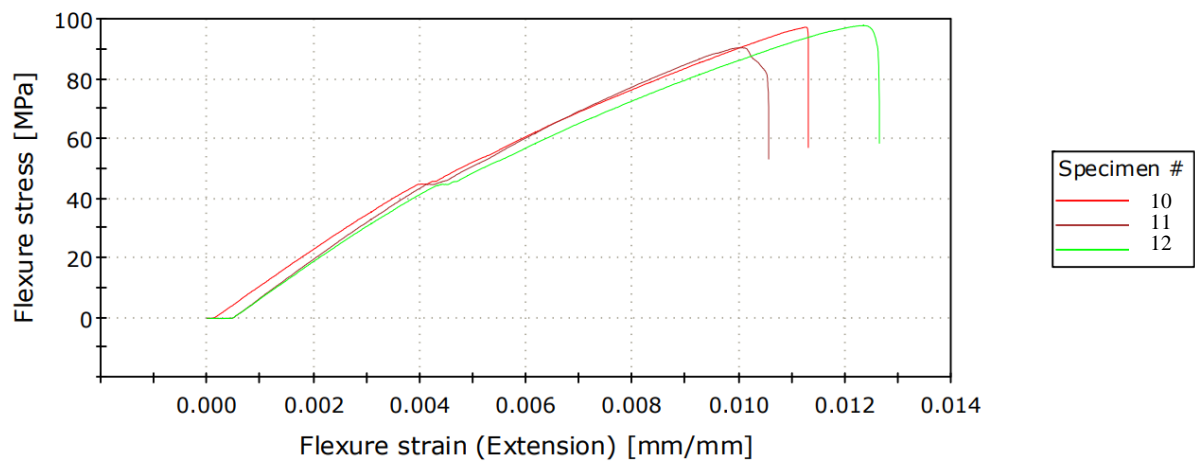


Figure 41: Flexural Tests for Coupons 10 to 12

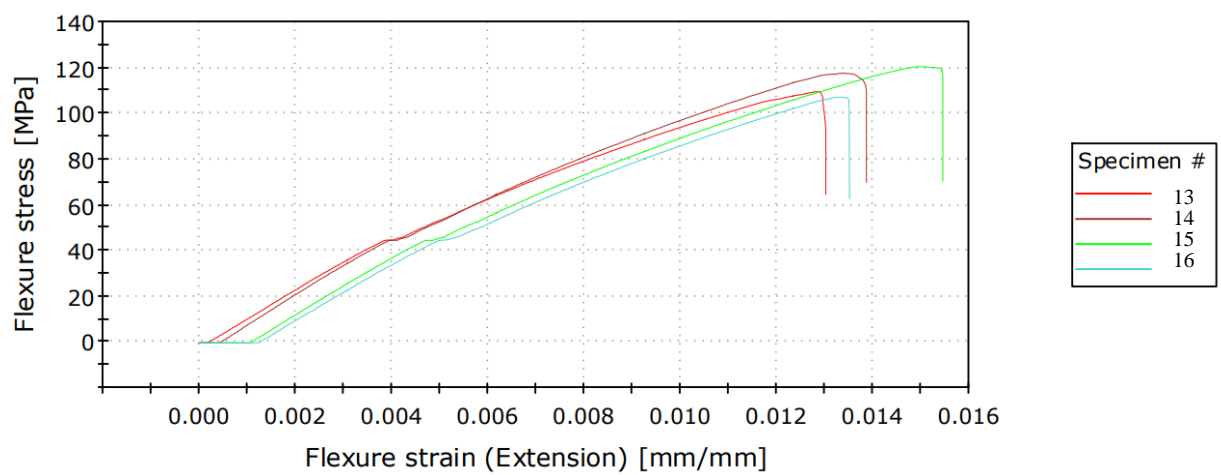


Figure 42: Flexural Tests for Coupons 13 to 16

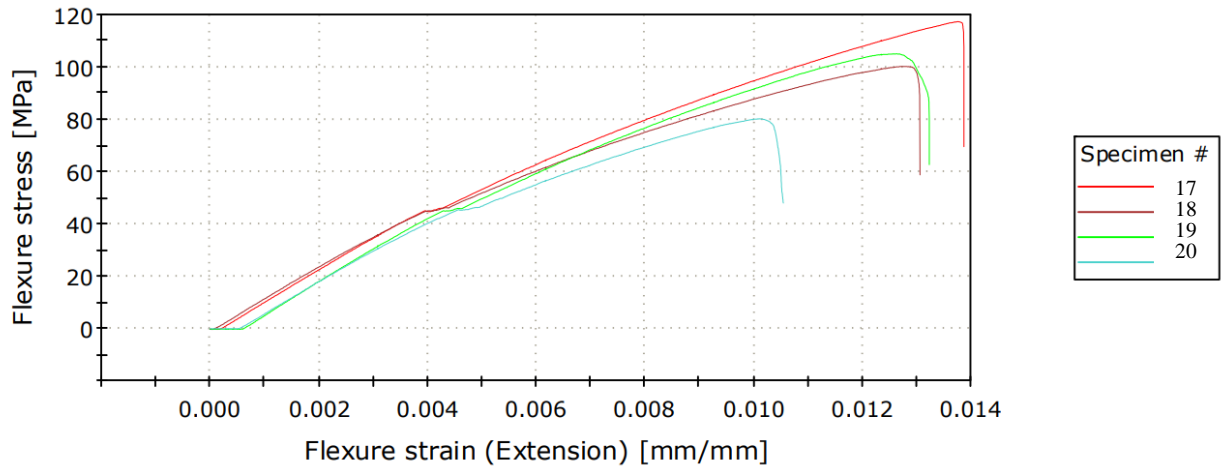


Figure 43: Flexural Tests for Coupons 17 to 20

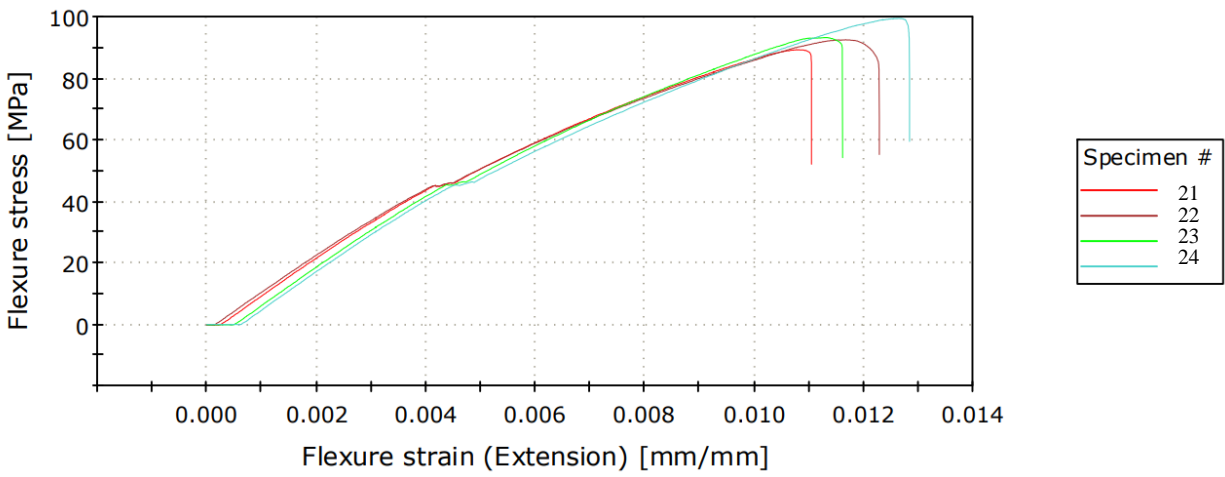


Figure 44: Flexural Tests for Coupons 21 to 24

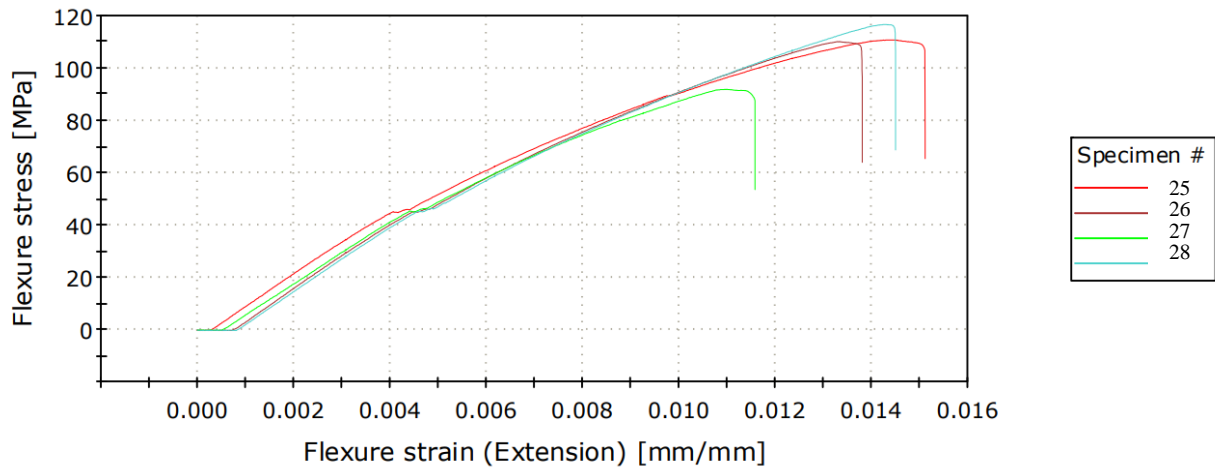


Figure 45: Flexural Tests for Coupons 25 to 28

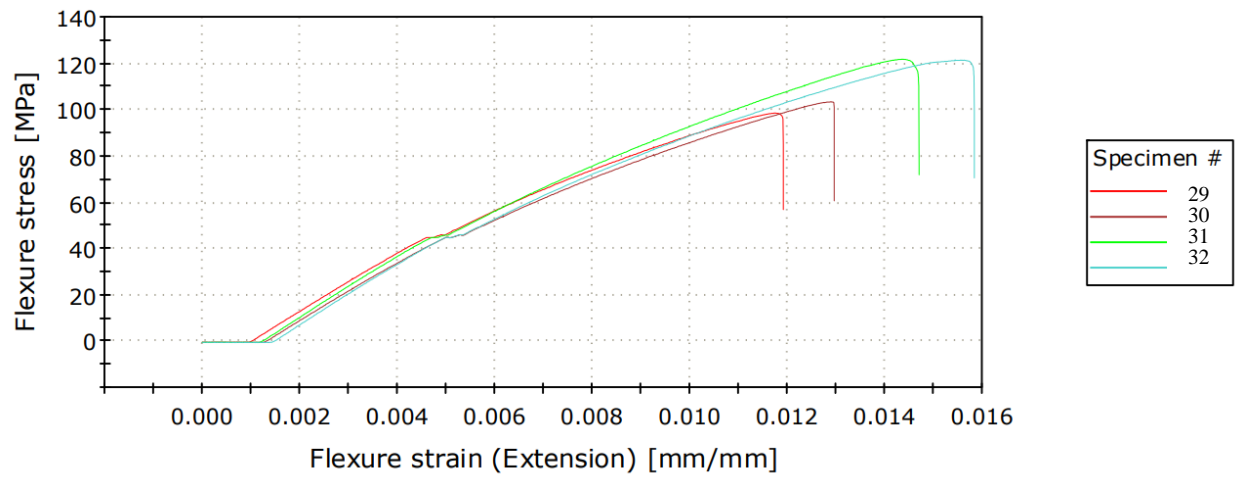


Figure 46: Flexural Tests for Coupons 29 to 32

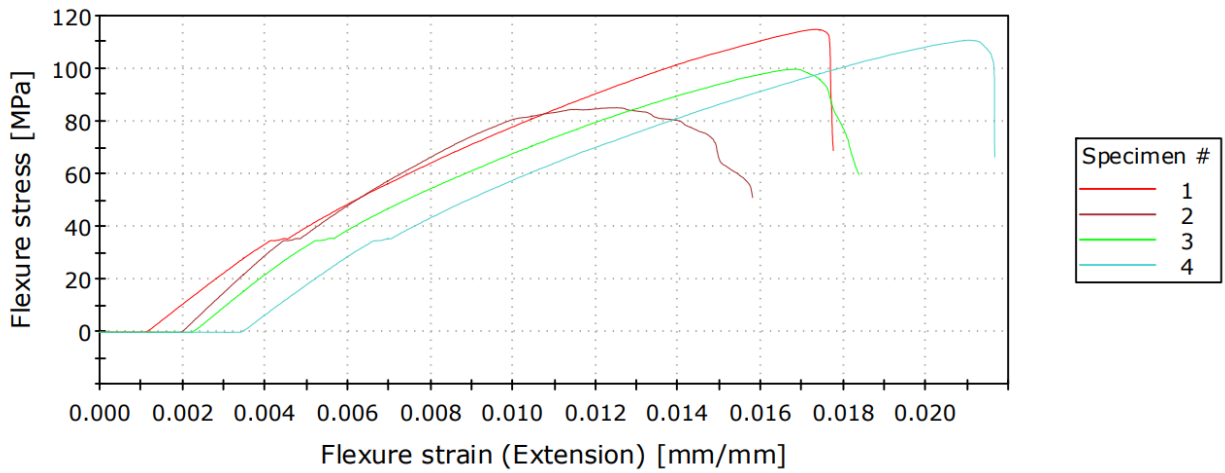


Figure 47: Flexural Tests for Plate 1 – 4 specimens

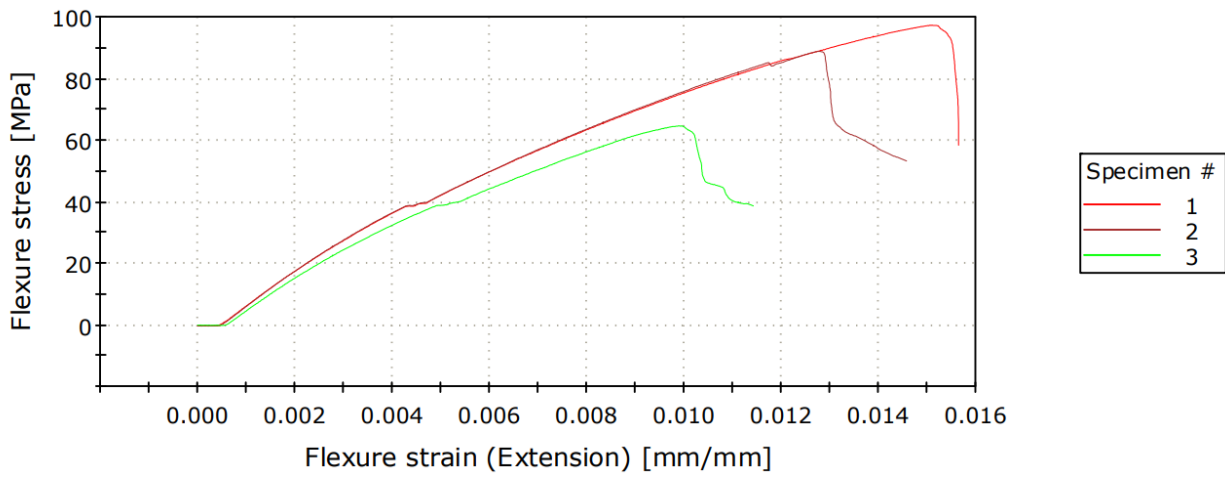


Figure 48: Flexural Tests for Plate 2 – 3 specimens

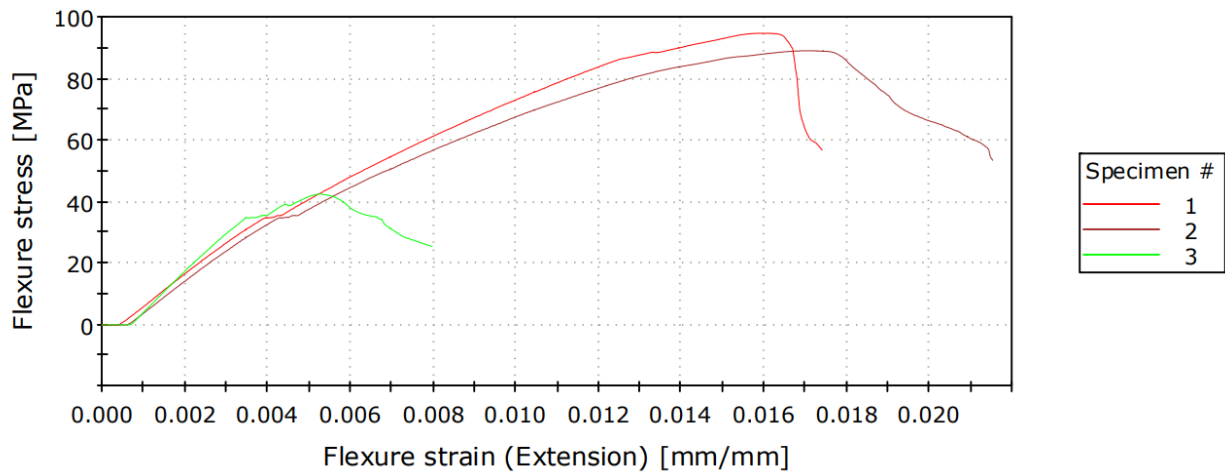


Figure 49: Flexural Tests for Plate 3 – 3 specimens

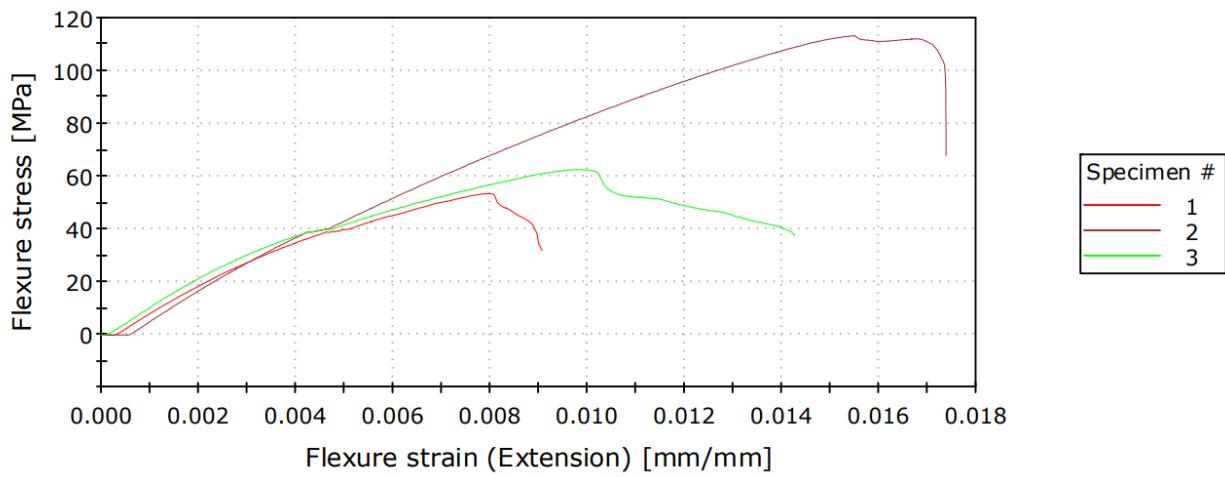


Figure 50: Flexural Tests for Plate 4 – 3 specimens

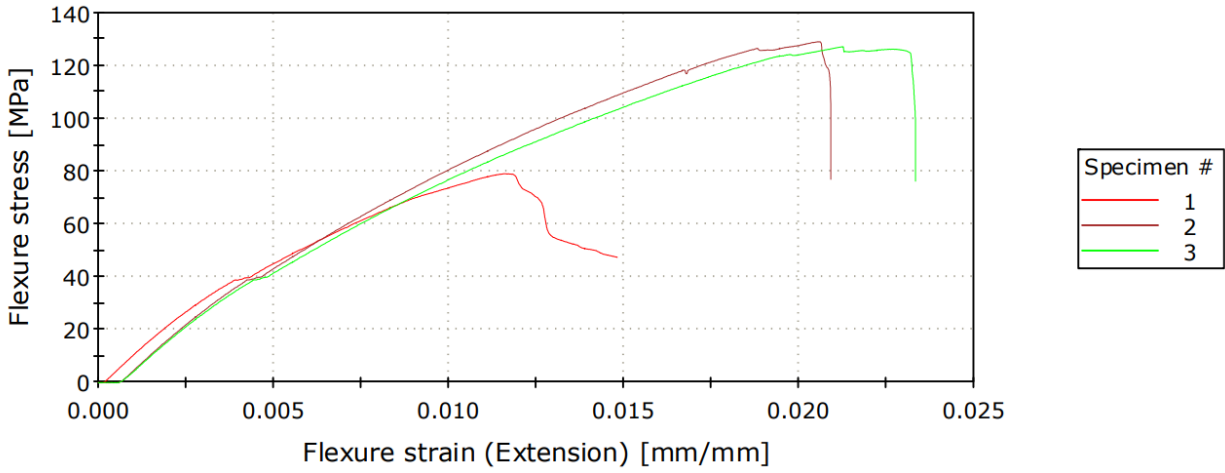


Figure 51: Flexural Tests for Plate 5 – 3 specimens

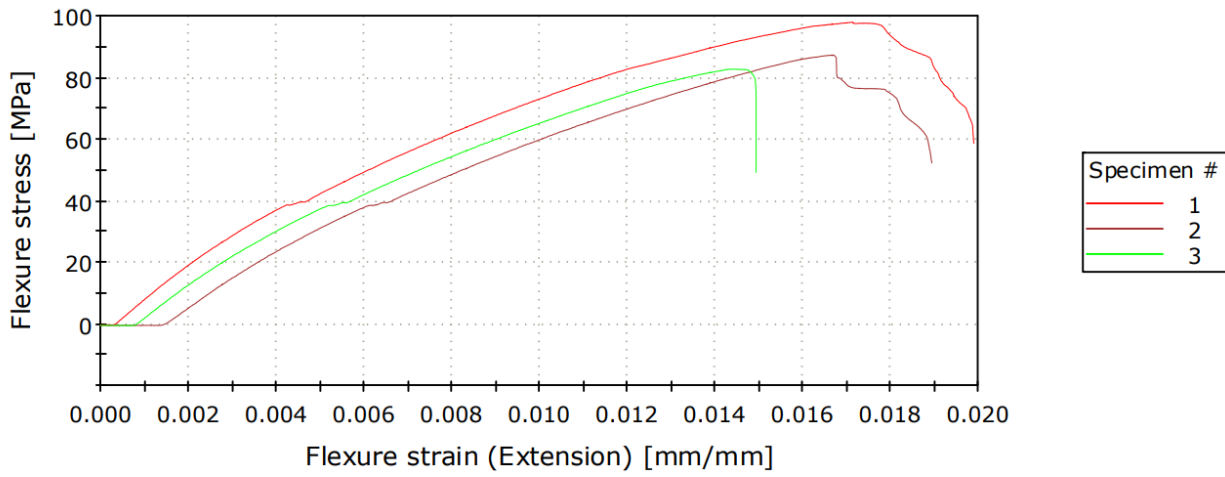


Figure 52: Flexural Tests for Plate 6 – 3 specimens

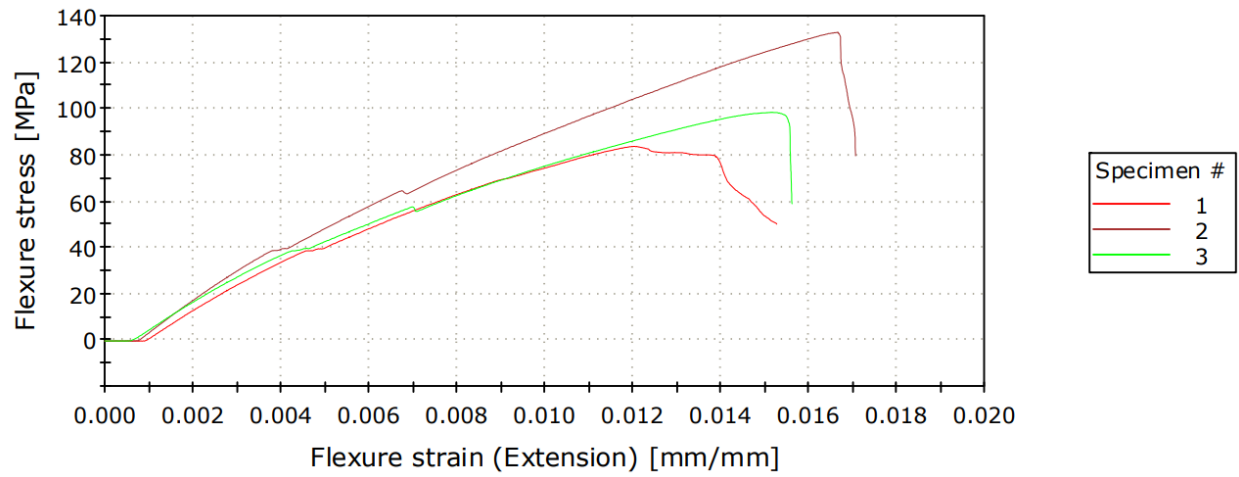


Figure 53: Flexural Tests for Plate 7 – 3 specimens

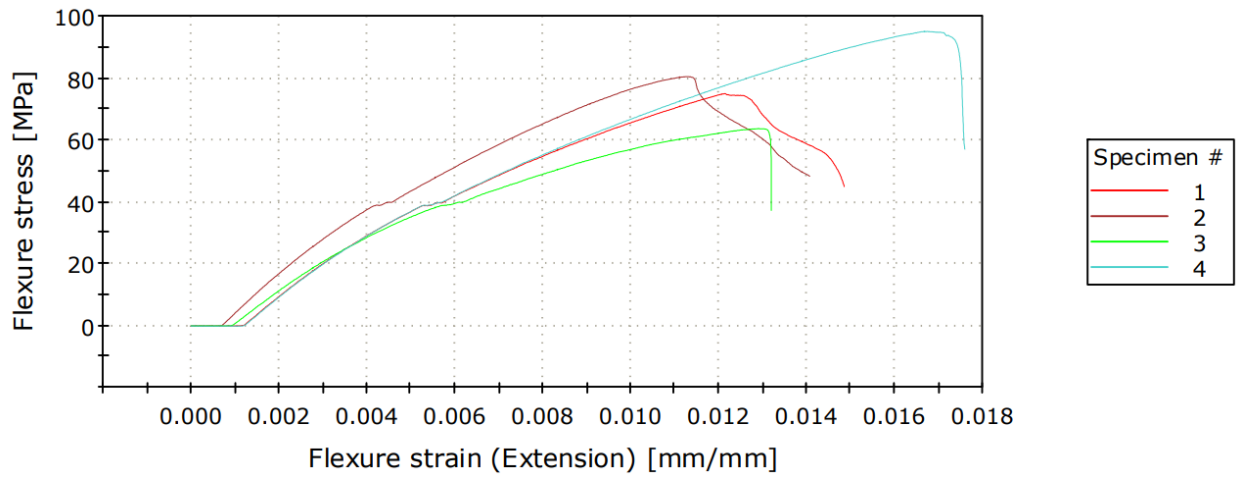


Figure 54: Flexural Tests for Plate 8 – 4 specimens

BIOGRAPHICAL SKETCH

Roberto Andres Garcia was born February 6, 1994 in McAllen, TX to Robert John Garcia and Sonia Martinez. He attended school in the Science Academy of South Texas until 2012, and began his college career at the University of Texas at Austin that fall. Aerospace wasn't all it cracked up to be and Rob ultimately completed an undergraduate degree in mechanical engineering at the University of Texas Rio Grande Valley in the fall of 2019. He graduated with a Master's degree in engineering with a concentration in mechanical engineering in the spring of 2022. While at UTRGV, he served as a research assistant on the University Transportation Center for Railway Safety team for three years and as a teaching assistant for an undergraduate course. Rob can be reached at robgarcia2112@gmail.com.